Progress In Electromagnetics Research, PIER 66, 317–357, 2006

UNIFIED SPECTRAL TECHNIQUE APPLICATION FOR STUDY OF RADIATOR BEHAVIOR NEAR PLANAR LAYERED COMPOSITES

M. Y. Koledintseva

University of Missouri-Rolla
1870 Miner Circle, Rolla, Missouri 65409-0040, USA

V. V. Bodrov, I. V. Sourkova, M. M. Sabirov and V. I. Sourkov

Moscow Power Engineering Institute
Technical University
14 Krasnokazarmennaya St., Moscow 111250, Russia

Abstract—The Unified Spectral Technique (UST) is a rigorous analytical approach for calculating power fluxes of any type of source and losses in multilayered dielectric structures of canonical geometries. This method is a reasonable addition to the eigenfunctions technique. An important advantage of the method is that the power fluxes are represented in an explicit form via their spectra, avoiding cumbersome calculations via field components. In this paper, this approach is specified for a case of planar multilayered structures, including those made of composite materials. Results of computations for the simplest types of radiators (electric and magnetic dipoles) in proximity of parallel-plane composite layers, comprised of a dielectric base and conducting inclusions with concentrations below and above percolation threshold, are analyzed.

1. INTRODUCTION

Practical interest for studying electromagnetic interaction of different radiators with composite layered structures both in far- and near-field zones has increased in recent years. In particular, these problems arise at the development of radomes to protect antenna systems, as well as shielding enclosures of different electronic devices to solve problems related to electromagnetic immunity.

It is important that frequency characteristics of material for radomes or shields would satisfy requirements, depending on particular application. In [1], the concept of engineering composites with the desired frequency response based on a genetic algorithm and effective medium theory, in particular, Maxwell Garnett formulation, has been developed for microwave shielding applications. The genetic algorithm optimization applied to combinations of composite layers with periodic 2D metafilm structures is considered in [2]. Sources of radiation acting upon layered structures are not necessarily in the far-field zone. In fact, they might be close to a structure under consideration, while the concepts of reflection and transmission coefficients, as well as of polarization and angles of incidence, are applicable only to the far-field region.

In the past decades, the effects of a presence of a dielectric layer on the radiation characteristics of antenna systems for various configurations have been intensively studied analytically and/or numerically, e.g., [3–10]. Modern full-wave numerical electromagnetic codes and specialized systems of computer-aided antenna and microwave/RF design allow for solving many complex problems. However, they require tremendous computer resources even when analyzing operation of relatively simple configurations of radiators in presence of dielectric structures in near and intermediate field regions. For this reason, it is still important to develop adequate analytical models to describe interaction of radiators with layered structures, since it may substantially reduce computer resources needed for the design of systems and structures of interest.

In the 1990's, the *Unified Spectral Technique* (UST) was proposed [11–14]. The UST is a generalized analytical method for arbitrary sources of radiation and any canonical geometry of dielectric layers — planar, cylindrical, and spherical. Spectra of electric and magnetic fields are calculated rigorously through scalar potentials using the known solutions of corresponding boundary problems. This approach for finding scalar potentials combines the known classical methods and includes the following stages:

- The scalar potentials for the geometry under consideration are derived using the approach in [4].
- The radiated fields are expanded as a Fourier series using a complete set of eigenfunctions of every structure along the coordinate axis parallel to the boundary.
- The source-like Cauchy representation of the radiated field along the coordinate axis normal to the boundary is applied.
- The analogy with circuit theory is used to reduce the complicated boundary problem to a single boundary condition.

The advantage of using the UST is that the power fluxes are represented in an explicit form via field spectra, rather than their field components, and this makes calculations less cumbersome. The standard approach developed in many publications, e.g., [3–10], is based on calculating components of the electric and the magnetic fields in layered structures. Calculation through fields demands the double integration of the E-component, double integration of the H-component, and double integral of the Poynting vector [4, 5]. Overall, it is necessary to calculate six integrals. It becomes especially cumbersome when the geometry of the radiator is complex. Using the UST, the order of integration is reduced only to a double integral for the plane case [11]; to a single integral and series for the cylindrical case [12]; and to a double series for the spherical case [13]. This is done by applying the Plancherel theorem [15]. Besides, the integrals are taken of the slowly varying functions of field spectra, but not of the fields containing rapidly varying exponents. This is important for assuring computational stability.

The UST is favorable for explicit calculation of the power fluxes in multilayered structures, when each layer is characterized by its effective electromagnetic parameters — permittivity and/or permeability. In the near-field zone, it is not always possible to separate contributions of reflected and transmitted fields or wave modes, and, hence it is reasonable to consider power fluxes instead of fields. The power fluxes will take into account energy of propagating waves, both backscattered and transmitted through layered structures, as well as electromagnetic energy loss due to such effects as excitation of evanescent waves, whose mode structure is not sustained by the geometry under consideration, scattering, and different mechanisms of ohmic or polarization loss and energy transformation. As for surface waves, they are also taken into account, since the UST is a rigorous full-wave formulation. However, surface waves appear only over a limited range of angles.

The objective of this paper is to apply the UST for calculating power characteristics of radiators (in particular, the radiation and absorption efficiencies) for analysis of planar layered structures that may contain composites. According to this formulation, the radiators may be of any type and complexity. For simplicity, in this paper only the cases of elementary electric and magnetic dipoles placed parallel to the boundary plane are considered. Multilayered structures can be treated using the cascading of classical transmission, or ABCD, matrices [16]. Recently, a paper on power absorption phenomena in near-field regions treated using a modal-based equivalent junction/circuit model [17] was published. In our paper, spectral densities of the introduced scalar electric and magnetic potentials also

resemble voltages and currents, similar to the equivalent circuit model.

The algorithm presented herein allows for calculating power fluxes in any media-lossless or lossy, including composite materials, both dielectrics and poor conductors. When media are lossless, the calculations are simplified. Since the fluxes through lossless media are independent of the coordinate normal to the boundaries, the corresponding power fluxes through any cross-section can be calculated as fluxes through the boundary, where the field spectra can be found in the simplest way.

The approach and analysis presented in this paper may be useful for the design of electromagnetic shields, and for taking into account parasitic electromagnetic coupling inside an electronic module, where there are many chips and other active elements as sources of radiation. The technique also can be generalized for the case of a two-dimensional array of radiators, which would be useful for the design of frequency-selective surfaces.

The structure of the paper is the following. Section 2 contains the mathematical background, where the UST is specified for a planar case. Some computational results in a planar layered geometry and for the simplest types of radiators, elementary electric and magnetic dipoles, are represented in Section 3. This section contains examples of computations for dielectric and conducting composite media. The effect of conductivity of inclusions, their geometry, and concentration on the absorption and radiation efficiency of a radiator near composite layers is studied. Some of the obtained results are compared with full-wave FDTD simulations. A discussion of the results and main conclusions are represented in Section 4. *Appendices A* and *B* contain the formulations of the problem for cylindrical and spherical geometries, respectively, and *Appendix C* contains the formulations for mixing rules for calculating effective permittivity of dielectric and conducting composites comprised of a dielectric base and conducting inclusions.

2. ELECTROMAGNETIC MODEL FOR CALCULATING POWER FLUXES

One of the objectives of this paper is to develop a model that allows for studying the behavior of radiators in proximity of shielding structures and giving a tool to engineer shielding materials with desirable electromagnetic parameters. As is known, the most important characteristic of any shielding enclosure is its shielding effectiveness (S.E.), associated with the level of attenuation of the electromagnetic field produced by the enclosure [18]. When near fields are taken into

account, it is reasonable to characterize shielding effectiveness in terms of power rather than fields, and to introduce the notions of absorption and radiation efficiencies in terms of electromagnetic power fluxes, as is done in [14].

Taking into account the power balance law, the absorption and radiation efficiencies calculated in the dimensionless form are related as

$$\eta_{\text{rad}} + \eta_{\text{abs}} = 1. \tag{1}$$

The absorption efficiency is defined as a ratio of the power flux lost in the structure to the power flux produced by the source.

$$\eta_{\text{abs}} = \frac{P_{\text{loss}}}{P_{\text{source}}}. \tag{2}$$

Then the radiation efficiency is found from (2),

$$\eta_{\text{rad}} = \frac{P_{\text{source}} - P_{\text{loss}}}{P_{\text{source}}}. \tag{3}$$

If the source is placed in a lossless medium, then $P_{\text{loss}} = P_{\text{abs}}$, the power flux absorbed by the material of the shielding enclosure, and $P_{\text{source}} = P_{\text{rad}}$, the total radiated power flux. Defined as (3), the radiation efficiency is associated with the total contribution of the "reflected" and "transmitted" power fluxes that might be difficult to separate when considering the near fields of radiators.

It should be mentioned that in practical electromagnetic engineering applications it may be reasonable to calculate the absorption and radiation efficiencies in decibels,

$$\begin{aligned} \eta_{\text{rad}}[\text{dB}] &= 10\log_{10}\frac{P_{\text{source}} - P_{\text{loss}}}{P_{\text{source}}}; \\ \eta_{\text{abs}}[\text{dB}] &= 10\log_{10}\frac{P_{\text{loss}}}{P_{\text{source}}}. \end{aligned} \tag{4}$$

To calculate the efficiencies η_{rad} and η_{abs}, it is necessary to calculate the power flux loss P_{loss} and the radiated power P_{rad}.

The geometries under consideration are shown in Figures 1–3. An impressed source having a volume current density $\vec{J}^{e,m}$ is placed arbitrarily under the dielectric layers of plane, cylindrical and spherical shapes, respectively. Power fluxes through the cross-sections z_i, r_i, or R_i, respectively, are

$$P_\alpha = \iint\limits_s \vec{p}_\alpha d\vec{S}, \tag{5}$$

where $\vec{p}_\alpha$ are the components of Poynting vector, and the coefficient α denotes z, r, or R. For the planar case, shown in Figure 1, the loss and radiated power fluxes are

$$\begin{aligned} P_{\text{loss}} &= P^+_{\text{rad}} - P^+_{tr} = P_{Z1} - P_{Z3}; \\ P_{\text{rad}} &= P^+_{\text{rad}} + P^-_{\text{rad}} = P_{Z1} + P_{Z2}. \end{aligned} \tag{6}$$

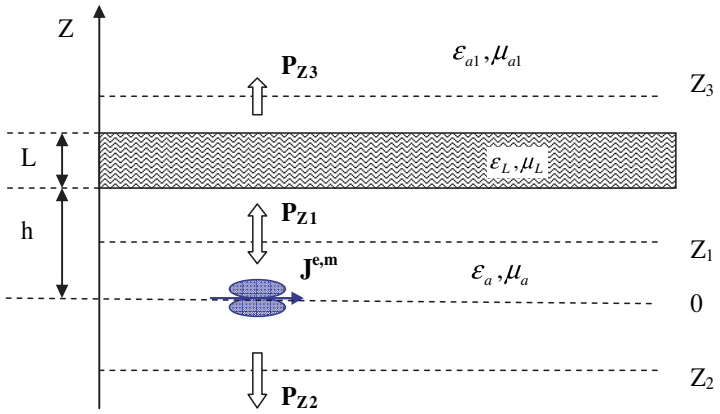

Figure 1. Parallel-plane layered dielectric structure.

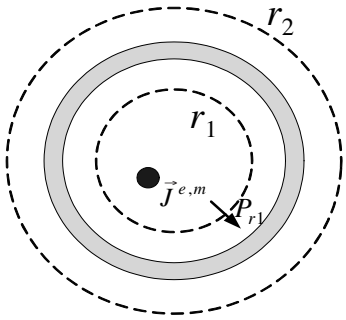

Figure 2. Cylindrical layered dielectric structure.

For the cylindrical case, shown in Figure 2, the power fluxes are

$$\begin{aligned} P_{\text{loss}} &= P_{r1} - P_{r2}; \\ P_{\text{rad}} &= P_{r2}. \end{aligned} \tag{7}$$

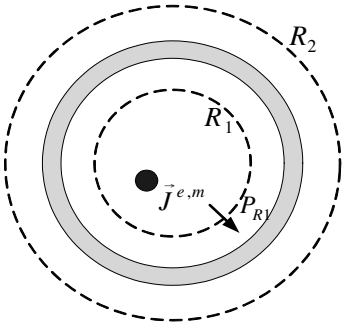

Figure 3. Spherical layered dielectric structure.

and for the spherical case, shown in Figure 3, the power fluxes are

$$\begin{aligned} P_{\text{loss}} &= P_{R1} - P_{R2}; \\ P_{\text{rad}} &= P_{R2}. \end{aligned} \tag{8}$$

The z-component of the Poynting vector in the parallel-plane geometry shown in Figure 1 is

$$p_z = \frac{1}{2}\text{Re}(E_x H_y^* - E_y H_x^*). \tag{9}$$

The tangential components of electromagnetic field, can be written in terms of the auxiliary functions $\Phi^{e,m}$ and $\psi^{e,m}$, analogous to the Debye scalar potentials in [4]:

$$\begin{aligned} E_x &= \frac{\partial \psi^e}{\partial x} + \frac{\partial \psi^m}{\partial y}; \quad H_x = \frac{\partial \Phi^m}{\partial x} - \frac{\partial \Phi^e}{\partial y}; \\ E_y &= \frac{\partial \psi^e}{\partial y} - \frac{\partial \psi^m}{\partial x}; \quad H_y = \frac{\partial \Phi^m}{\partial y} + \frac{\partial \Phi^e}{\partial x}. \end{aligned} \tag{10}$$

The superscripts "e" and "m" stand for the waves of electric and magnetic types, respectively. It is convenient to represent these auxiliary scalar potentials $\Phi^{e,m}$ and $\psi^{e,m}$ as the Fourier integrals, according to the method of eigenfunctions,

$$\begin{aligned} \Phi^{e,m} &= \iint\limits_{\chi_1,\chi_2} I^{e,m} e^{-i\chi_1 x - i\chi_2 y} d\chi_1 d\chi_2; \\ \psi^{e,m} &= \iint\limits_{\chi_1,\chi_2} U^{e,m} e^{-i\chi_1 x - i\chi_2 y} d\chi_1 d\chi_2, \end{aligned} \tag{11}$$

where $I^{e,m}$ and $U^{e,m}$ are the spectral densities of the scalar potentials $\Phi^{e,m}$ and $\psi^{e,m}$, respectively. Then (10) can be represented as

$$\vec{E}_\tau = \iint\limits_{\chi_1\chi_2} \left(U^e\vec{t} + U^m\vec{f}\right) d\chi_1 d\chi_2; \quad \vec{H}_\tau = \iint\limits_{\chi_1\chi_2} \left(I^e\vec{t} + I^m\vec{f}\right) d\chi_1 d\chi_2, \tag{12}$$

where $(\vec{t};\ \vec{f})$ is the complete system of vector eigenfunctions

$$\begin{aligned} \vec{t} &= (-i\chi_1\vec{x}_0 - i\chi_2\vec{y}_0)\, e^{-i\chi_1 x - i\chi_2 y}; \\ \vec{f} &= (-i\chi_2\vec{x}_0 + i\chi_1\vec{y}_0)\, e^{-i\chi_1 x - i\chi_2 y}, \end{aligned} \tag{13}$$

expressed via the unit vectors in the Cartesian coordinate system $\vec{x}_0$ and $\vec{y}_0$.

The expression for the power flux is obtained by substituting (12) and (13) in (9):

$$P_z = 2\pi^2 \mathrm{Re}\left[\iint\limits_{\chi_1\chi_2} \chi^2 (U^e I^{e*} + U^m I^{m*}) d\chi_1 d\chi_2\right], \tag{14}$$

where $\chi^2 = \chi_1^2 + \chi_2^2$.

It is important that the spectral densities of the scalar potentials $I^{e,m}$ and $U^{e,m}$, used instead of the field components, play the part of the generalized "currents" and "voltages". The first term of (14) represents the power flux due to the electric field, and the second term is the flux due to the magnetic field. At this point, assume that the values $I^{e,m}$ and $U^{e,m}$ are known. However, it is necessary first to obtain them from the rigorous solution of the corresponding boundary problem, taking into account physical effects of diffraction, absorption, refraction, and numerous reflections. Substitution of the Fourier representation for the field components (12) in Maxwell's equations leads to the differential equations of the 2nd order with respect to $I^{e,m}$ and $U^{e,m}$. In the areas of the existence of the reflected waves, that is, in the cross-sections z_1 and z_2, and within the dielectric layers (see Figure 1), the solution for $I^{e,m}$ and $U^{e,m}$ is the following

$$\begin{aligned} U^{e,m} &= U_{in}^{e,m} + U_r^{e,m}, \\ I^{e,m} &= \left(U_{in}^{e,m} - U_r^{e,m}\right)/Z^{e,m}, \end{aligned} \tag{15}$$

where $U_{in}^{e,m}$ and $U_r^{e,m}$ are in the form of propagating waves with the exponential terms $e^{-\gamma z}$ and $e^{+\gamma z}$, respectively. The values γ and $Z^{e,m}$ are the propagation constant and the characteristic impedance

in the cross-section z under consideration, respectively, as shown in Figure 4. The amplitudes $U_{in}^{e,m}$ and $U_r^{e,m}$ in (15) are the coefficients of two linearly independent solutions for the one-dimensional Helmholtz equation with the appropriate boundary conditions; the index "in" corresponds to the "incident" waves propagating in the positive direction of the axis z, and the index "r" stands for the "reflected" waves propagating in the negative direction of the axis z. In the cross-section z_3, where the reflected waves are absent, the values $U_r^{e,m}$ and $J_r^{e,m}$ are equal to zero.

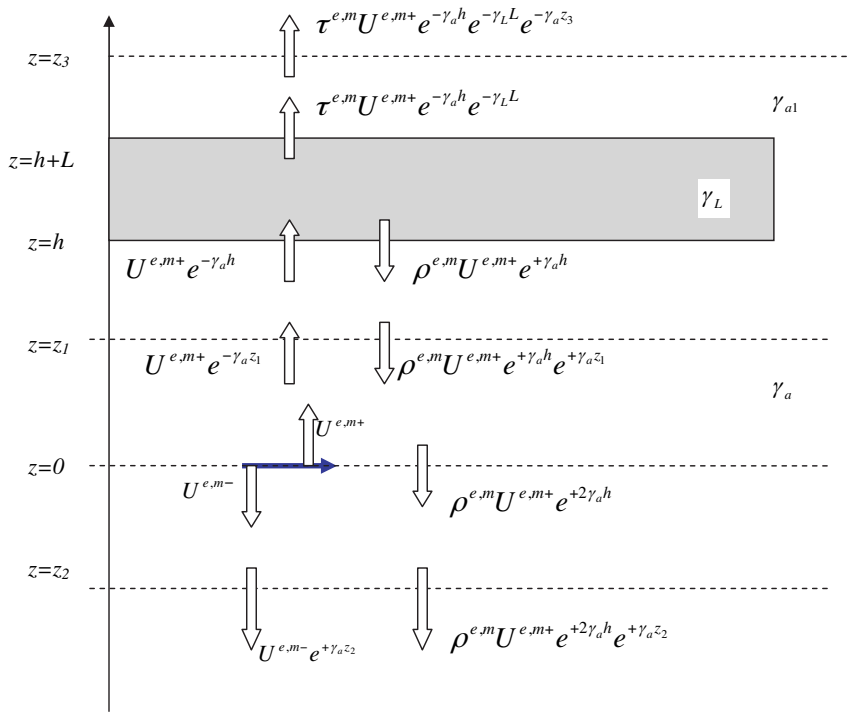

Figure 4. Power fluxes in a parallel-plane layered structure.

Let the impressed source be placed in any medium with, in the general case, complex absolute permittivity and permeability (ε_a, μ_a). Then, the corresponding propagation constant is $\gamma_a^2 = \chi^2 - k_a^2$, where $\chi^2 = \chi_1^2 + \chi_2^2$, and $k_a = \omega\sqrt{\varepsilon_a \mu_a}$. The values $Z_a^{e,m}$ are the characteristic impedances of the medium for the waves of electric (e) or magnetic (m)

types, respectively,

$$Z_a^e = \frac{\gamma_a}{i\omega\varepsilon_a}; \quad Z_a^m = \frac{i\omega\mu_a}{\gamma_a}. \tag{16}$$

Suppose, for simplicity, that the medium with the parameters (ε_a, μ_a) is lossless. Then the wave number k_a is real and positive. The power flux through the cross-section z_1 will be considered for two cases: (a) $|\chi| < k_a$ and (b) $|\chi| \geq k_a$, corresponding to the contributions of propagating and evanescent waves, respectively.

(a) When $|\chi| < k_a$, the propagation constant $\gamma_a = i\beta_a$ is imaginary, and the characteristic impedance $Z_a^{e,m}$ is real. Then the power flux is found as

$$P_{z\,\mathrm{prop}} = 2\pi^2 \iint\limits_{\chi_1\chi_2} \chi^2 \left[\frac{|U_{in}^e|^2 - |U_r^e|^2}{Z_a^e} + \frac{|U_{in}^m|^2 - |U_r^m|^2}{Z_a^m} \right] d\chi_1 d\chi_2. \tag{17}$$

(b) When $|\chi| \geq k_a$, the propagation constant γ_a is real, the characteristic impedance $Z_a^{e,m} = iX_a^{e,m}$ is imaginary, and the power flux is

$$P_{z\,\mathrm{evan}} = 4\pi^2 \iint\limits_{\chi_1\chi_2} \chi^2 \left[\frac{\mathrm{Im}(U_{in}^e U_r^{e*})}{X_a^e} + \frac{\mathrm{Im}(U_{in}^m U_r^{m*})}{X_a^m} \right] d\chi_1 d\chi_2. \tag{18}$$

As mentioned above, the exact expressions for the coefficients $U_{in}^{e,m}$ and $U_r^{e,m}$ should be known for the given boundary conditions and the given sources.

At this point, two important conclusions can be derived.

The first conclusion is the independence of the coefficients $U_{in}^{e,m}$ and $U_r^{e,m}$ on the z-coordinate for a lossless medium. Therefore, the power flux through the surface that crosses a medium without loss is also independent of the z-coordinate. Hence, a power flux through any cross-section can be calculated as a flux through the boundary, where the field spectra can be found in the simplest way.

The second conclusion is that any calculated power flux can be comprised of two terms: the first term (17) is determined by the propagating waves when $\gamma_a = i\beta_a$, and the second term (18) is determined by evanescent, or non-propagating waves when γ_a is real. Only for the regions where there are no reflected fields, that is, $U_r^{e,m} = 0$ and $J_r^{e,m} = 0$, the power flux is determined only by propagating waves.

Consider power fluxes through three cross-sections shown in Figure 4.

1) Cross-section z_1. There are both incident and reflected waves, so that

$$\begin{aligned} U_{in}^{e,m}(z_1) &= U^{e,m+}e^{-\gamma_a z_1}; \\ U_r^{e,m}(z_1) &= U^{e,m-}e^{+\gamma_a z_1} = \rho^{e,m}\cdot U^{e,m+}\cdot e^{\gamma_a(h+z_1)}, \end{aligned} \tag{19}$$

where $\rho^{e,m}$ is the reflection coefficient at the boundary $z = h$ given below in (34). The total power flux that includes powers of all propagating and evanescent waves is

$$P_z(z_1) = P^e_{z\,\mathrm{prop}}(z_1) + P^m_{z\,\mathrm{prop}}(z_1) + P^e_{z\,\mathrm{evan}}(z_1) + P^m_{z\,\mathrm{evan}}(z_1). \tag{20}$$

The power flux of propagating waves in a lossless medium (ε_a, μ_a) is

$$P^{e,m}_{z\,\mathrm{prop}}(z_1) = 2\pi^2 \iint\limits_{\chi_1\chi_2} \chi^2 \left[\frac{\left|U^{e,m+}e^{-\gamma_a z_1}\right|^2 - \left|\rho^{e,m}U^{e,m+}e^{\gamma_a(h+z_1)}\right|^2}{Z_a^{e,m}}\right] d\chi_1 d\chi_2; \quad |\chi| < k_a \tag{21}$$

The power flux of evanescent waves is

$$P^{e,m}_{z\mathrm{evan}}(z_1) = 4\pi^2 \iint\limits_{\chi_1\chi_2} \chi^2 \frac{|U^{e,m+}|^2 \cdot \mathrm{Im}\left(\rho^{e,m}e^{-\gamma_a z_1}e^{(-j\beta_a+\alpha_a)(h+z_1)}\right)}{X_a^{e,m}} d\chi_1 d\chi_2; \quad |\chi| \geq k_a. \tag{22}$$

If the medium (ε_a, μ_a) is lossy, then the propagation constant is complex, $\gamma_a = \alpha_a + j\beta_a$.

2) Cross-section z_2: There is only one wave propagating in the negative direction of the z axis,

$$\begin{aligned} U_{in}^{e,m}(z_2) &= 0; \\ U_r^{e,m}(z_2) &= U^{e,m-}e^{+\gamma_a z_2} + U^{e,m+}\cdot\rho^{e,m}\cdot e^{\gamma_a(2h+z_2)}. \end{aligned} \tag{23}$$

The power flux in this cross-section is calculated using the formula

$$P^{e.m}_{z\,\mathrm{prop}}(z_2) = 2\pi^2 \iint\limits_{\chi_1\chi_2} \chi^2 \left[\frac{\left|U^{e,m-}e^{+\gamma_a z_2} + \rho^{e,m}U^{e,m+}e^{\gamma_a(2h+z_2)}\right|^2}{Z_a^{e,m}}\right] d\chi_1 d\chi_2; \quad |\chi| < k_a \tag{24}$$

3) Cross-section z_3: There is only the propagating wave in the positive direction of the axis z

$$U_{in}^{e,m}(z_3) = \tau^{e,m}\cdot U^{e,m+}\cdot e^{-\gamma_a h}e^{-\gamma_L L}e^{-\gamma_{a1} z_3}; \quad U_r^{e,m}(z_3) = 0, \tag{25}$$

where γ_L is the propagation constant within the dielectric layer of thickness L. If this is a multilayer structure, then γ_L is an equivalent propagation constant calculated through cascading of the layers. In (25), $\tau^{e,m}$ is the transmission coefficient. It is calculated as is given below in (32).

Then the flux of propagating waves in this cross-section (z_3) can be calculated as

$$P^{e,m}_{z\text{prop}}(z_3) = 2\pi^2 \iint\limits_{\chi_1\chi_2} \chi^2 \frac{\left|U^{e,m+}\right|^2 \cdot \left|\tau^{e,m} e^{-\gamma_a h} e^{-\gamma_L L} e^{-\gamma_{a1} z_3}\right|^2}{Z^{e,m}_{a1}} d\chi_1 d\chi_2; \quad |\chi| < k_a. \tag{26}$$

Using the relations (15), one can relate "voltages" and "currents" ($U^{e,m}_n$, $I^{e,m}_n$) on the upper boundary of a layer number n with "voltages" and "currents" ($U^{e,m}_{n-1}$, $I^{e,m}_{n-1}$) on the lower boundary of the layer, using the transmission matrix $[A]^{e,m}_n = \begin{bmatrix} a^{e,m}_n & b^{e,m}_n \\ c^{e,m}_n & d^{e,m}_n \end{bmatrix}$,

$$\begin{bmatrix} U^{e,m}_{n-1} \\ I^{e,m}_{n-1} \end{bmatrix} = [A]^{e,m}_n \cdot \begin{bmatrix} U^{e,m}_n \\ I^{e,m}_n \end{bmatrix}. \tag{27}$$

The elements of the transmission matrix for any dielectric layer of thickness l_n are

$$\begin{aligned} a^{e,m}_n &= d^{e,m}_n = \cosh(\gamma_n l_n); \\ b^{e,m}_n &= Z^{e,m}_n \sinh(\gamma_n l_n); \\ c^{e,m}_n &= \frac{1}{Z^{e,m}_n} \sinh(\gamma_n l_n). \end{aligned} \tag{28}$$

where the complex propagation constant γ_n and characteristic impedance $Z^{e,m}_n$ are determined by the constitutive parameters of the layer ε_n and μ_n. Then, the relation between the values ($U^{e,m}_N$, $I^{e,m}_N$) at the final boundary and ($U^{e,m}_0$, $I^{e,m}_0$) at the very first boundary is the cascading of the transmission matrices,

$$\begin{bmatrix} U^{e,m}_0 \\ I^{e,m}_0 \end{bmatrix} = [A]^{e,m}_1 \cdot [A]^{e,m}_2 \cdot \ldots \cdot [A]^{e,m}_N \cdot \begin{bmatrix} U^{e,m}_N \\ I^{e,m}_N \end{bmatrix}. \tag{29}$$

From the theory of 2-port devices [16], one can calculate the input impedance at the lower (initial) cross-section as

$$Z^{e,m}_{in0} = \frac{a^{e,m} Z^{e,m}_a + b^{e,m}}{c^{e,m} Z^{e,m}_a + d^{e,m}}, \tag{30}$$

where $a^{e,m}$, $b^{e,m}$, $c^{e,m}$, and $d^{e,m}$ are the parameters of the resultant transmission matrix $[A]^{e,m} = \prod_{n=1}^{N} [A]_n^{e,m}$.

If the upper half-space has the characteristic impedance $Z_{a1}^{e,m} \neq Z_a^{e,m}$, then the reflection and transmission coefficients are

$$\rho^{e,m} = \frac{Z_{in0}^{e,m} - Z_{a1}^{e,m}}{Z_{in0}^{e,m} + Z_{a1}^{e,m}} = \frac{(a^{e,m} Z_a^{e,m} + b^{e,m}) - Z_{a1}^{e,m}(c^{e,m} Z_a^{e,m} + d^{e,m})}{(a^{e,m} Z_a^{e,m} + b^{e,m}) + Z_{a1}^{e,m}(c^{e,m} Z_a^{e,m} + d^{e,m})}, \quad (31)$$

and

$$\tau^{e,m} = \frac{2Z_{a1}^{e,m}}{Z_{in0}^{e,m} + Z_{a1}^{e,m}} = \frac{2Z_{a1}^{e,m}}{(a^{e,m} Z_a^{e,m} + b^{e,m}) + Z_{a1}^{e,m}(c^{e,m} Z_a^{e,m} + d^{e,m})}. \quad (32)$$

In the particular case, when the upper half-space is the same as below the multilayered structure, $Z_a^{e,m} = Z_{a1}^{e,m}$, the reflection coefficient is calculated as

$$\rho^{e,m} = \frac{a^{e,m} - d^{e,m} + b^{e,m}/Z_a^{e,m} - c^{e,m} Z_a^{e,m}}{a^{e,m} + d^{e,m} + b^{e,m}/Z_a^{e,m} + c^{e,m} Z_a^{e,m}}, \quad (33)$$

and the transmission coefficient is

$$\tau^{e,m} = \frac{2}{a^{e,m} + b^{e,m}/Z_a^{e,m} + c^{e,m} Z_a + d^{e,m}}. \quad (34)$$

Amplitudes $U^{e,m\pm}$ depend on the type and orientation of the radiator under consideration. If this is an elementary electric or magnetic dipole, the impressed currents are

$$J_{x,y,z}^{e,m} = j_{x,y,z}^{e,m} \cdot \delta(x - x_0) \cdot \delta(y - y_0) \cdot \delta(z - z_0), \quad (35)$$

where $j_{x,y,z}^{e,m}$ is the corresponding dipole moment of the radiator, and δ is the Dirac delta-function. According to Figure 4, the source is placed in the plane $z_0 = 0$.

The closed-form expressions for $U^{e,m\pm}$ for any cross-section z (with corresponding complex propagation constant γ_a in the medium, where the source is placed) can be obtained taking into account symmetry of the dielectric structure along the x and y axes. The dipoles oriented along x produce the same power fluxes as those oriented along y, and the corresponding expressions simplify.

$$U^{e\pm} = \frac{ie^{\pm\gamma_a z}}{8\pi^2 \chi^2} \cdot \left[-Z_a^e (\chi_1 a_x^e) \pm \left(\frac{a_z^e \chi^2}{\omega \varepsilon_0} + \chi_2 a_x^m \right) \right] \quad (36)$$

and

$$U^{m\pm} = \frac{ie^{\pm\gamma_a z}}{8\pi^2\chi^2} \cdot \left[Z_a^e \cdot \left(\frac{a_z^m \chi^2}{\omega\mu_0} - \chi_2 a_x^e \right) \mp \chi_1 a_x^m \right]. \tag{37}$$

From the above rigorous solution it is seen that the power flux contains the contribution of higher-order modes that transfer energy, when the reflection coefficient is non-zero. If the source is close to the surface, this contribution can be substantial.

Below there are given the explicit formulas for the calculation of power fluxes through the cross-sections z_1, z_2, and z_3, shown in Figures 1 and 4, when the source under consideration is an ***elementary electric dipole*** oriented along the x axis. It is assumed that the dielectric slab is surrounded by air.

The power flux $P_z(z_1)$ can be calculated using (21) and (22) as a double Fourier transform. To calculate these integrals, it is convenient to use the following substitutions:

$$\begin{aligned} \chi_1 &= \chi\cos\alpha; \\ \chi_2 &= \chi\sin\alpha; \\ d\chi_1 d\chi_2 &= \chi d\chi d\alpha, \end{aligned} \tag{38}$$

and then the integral with respect to α is calculated in an explicit form.

For real χ, it is convenient to introduce the notation $\chi = k_a\cos\theta$. Then the integral with respect to $|\chi| < k_a$, corresponding to the power fluxes of the propagating waves, should be calculated in the limits for $\theta \in (0; 2\pi)$. When $|\chi| \geq k_a$, the angles θ are imaginary, and the corresponding integral with respect to the imaginary angles describes the evanescent waves (i. e., γ_a is real).

This means that the power fluxes (21) and (22) are calculated as

$$P_z^{e,m} = \int\limits_{\chi=0}^{\infty} \ldots d\chi = \int\limits_{\theta=0}^{2\pi} \ldots d\theta + \int\limits_{\chi=k_a}^{\infty} \ldots d\chi. \tag{39}$$

To calculate evanescent power fluxes with respect to the imaginary angles, it is convenient to use the normalized propagation constant $\gamma_n = \gamma_L/k_a = \sqrt{y^2 + 1 - n^2}$ expressed through the newly introduced parameter y and the parameter $n^2 = \varepsilon_L/\varepsilon_a$, which is a ratio of permittivities of the dielectric layer and the surrounding space. When the dielectric layer is surrounded by air, $n = \sqrt{\varepsilon_r}$ is just the refractive

index of the dielectric layer. Then (39) transforms to

$$P_z^{e,m} = \int_{\theta=0}^{2\pi} \dots d\theta + \int_{y=0}^{\infty} \dots dy. \tag{40}$$

The corresponding power fluxes for propagating and evanescent waves through the cross-section z_1 are calculated as follows:

$$\begin{aligned}
P^m_{z\text{prop}}(z_1) &= \int_{\theta=0}^{\pi/2} \left(1 - \left|\rho^m_{\text{prop}}\right|^2\right) \sin\theta \cdot d\theta; \\
P^e_{z\text{prop}}(z_1) &= \int_{\theta=0}^{\pi/2} \cos^2\theta \left(1 - \left|\rho^e_{\text{prop}}\right|^2\right) \sin\theta \cdot d\theta; \\
P^m_{z\text{evan}}(z_1) &= \int_{y=0}^{\infty} (-2) \cdot \text{Im}(\rho^m_{\text{evan}}) \cdot e^{-4\pi h y} dy; \\
P^e_{z\text{evan}}(z_1) &= \int_{y=0}^{\infty} 2y^2 \cdot \text{Im}(\rho^e_{\text{evan}}) \cdot e^{-4\pi h y} dy.
\end{aligned} \tag{41}$$

In (41), $\rho^{e,m}_{\text{prop}}$ is the reflection coefficient for the propagating waves, and the notation $\rho^{e,m}_{\text{evan}}$ corresponds to the evanecsent waves, though in the prior formulation the notation $\rho^{e,m}$ was used for any kind of waves.

As is shown above, for the cross-sections z_2 and z_3, the resultant power flux P_z is comprised only of the contributions by the propagating waves. For the cross-section z_2 ,the power flux $P_z(z_2)$ is found as

$$\begin{aligned}
P_{z\text{prop}}(z_2) &= P^e_{z\text{prop}} + P^m_{z\text{prop}} \\
&= \int_{\theta=0}^{\pi/2} \left\{ \begin{array}{l} \cos^2\theta \left|1 + \rho^e_{\text{prop}} \cdot e^{-i4\pi \cdot h\cos\theta}\right|^2 + \\ \left|1 + \rho^m_{\text{prop}} \cdot e^{-i4\pi \cdot h\cos\theta}\right|^2 \end{array} \right\} \sin\theta d\theta.
\end{aligned} \tag{42}$$

For the cross-section z_3, the total power flux $P_z(z_3)$ can be written as

$$P_{z\text{prop}}(z_3) = P^e_{z\text{prop}} + P^m_{z\text{prop}} = \int_{\theta=0}^{\pi/2} \left\{\cos^2\theta \cdot |\tau^e|^2 + |\tau^m|^2\right\} \sin\theta d\theta. \tag{43}$$

When considering an ***elementary magnetic dipole*** oriented along the axis x, the power flux $P_z(z_1)$ is calculated using (20),

$$\begin{aligned}
P^e_{z\text{prop}}(z_1) &= \int\limits_{\theta=0}^{\pi/2} \left(1 - \left|\rho^e_{\text{prop}}\right|^2\right) \sin\theta d\theta; \\
P^m_{z\text{prop}}(z_1) &= \int\limits_{\theta=0}^{\pi/2} \cos^2\theta \left(1 - \left|\rho^m_{\text{prop}}\right|^2\right) \sin\theta d\theta; \\
P^e_{z\text{evan}}(z_1) &= \int\limits_{y=0}^{\infty} 2\text{Im}(\rho^e_{\text{evan}}) e^{-4\pi h y} dy; \\
P^m_{z\text{evan}}(z_1) &= \int\limits_{y=0}^{\infty} -2y^2 \cdot Im(\rho^m_{\text{evan}}) e^{-4\pi h y} dy.
\end{aligned} \tag{44}$$

The power flux $P_z(z_2)$ in the cross-section z_2 is found as

$$\begin{aligned}
&P_{z\text{prop}}(z_2) = P^e_{z\text{prop}} + P^m_{z\text{prop}} \\
&= \int\limits_{\theta=0}^{\pi/2} \left\{ \left|1 - \rho^e_{\text{prop}} \cdot e^{-i4\pi \cdot h\cos\theta}\right|^2 + \cos^2\theta \cdot \left|1 - \rho^m_{\text{prop}} \cdot e^{-i4\pi \cdot h\cos\theta}\right|^2 \right\} \sin\theta \cdot d\theta
\end{aligned} \tag{45}$$

In the cross-section z_3, the total power flux $P_z(z_3)$ can be written as

$$P_{z\text{prop}}(z_3) = P^e_{z\text{prop}} + P^m_{z\text{prop}} = \int\limits_{\theta=0}^{\pi/2} \left\{ |\tau^e|^2 + \cos^2\theta \cdot |\tau^m|^2 \right\} \sin\theta \cdot d\theta \tag{46}$$

To simplify the expressions for finding reflection and transmission coefficients in the formulas (41)–(46), it is convenient to introduce the notations

$$\begin{aligned}
G &= \sqrt{n^2 - \sin^2\theta}; \\
\phi &= 2\pi \cdot L \cdot G; \\
Q_y &= 2\pi L \gamma_n = 2\pi L \sqrt{y^2 + 1 - n^2},
\end{aligned} \tag{47}$$

where L is the thickness of the layer, and $n = \sqrt{\varepsilon_L/\varepsilon_a}$ is the relative refractive index. When the dielectric layer with the realtive

permittivity ε_r is surrounded by air, the refractive index equals to $n = \sqrt{\varepsilon_r}$.

Then the transmission coefficients for propagating waves, characterized by real angles, can be found using the formulas

$$\begin{aligned} \tau^m(\theta) &= \frac{2G \cdot \cos\theta}{2G \cdot \cos\theta \cdot \cos\phi + i \cdot \sin\phi \cdot (G^2 + \cos^2\theta)}; \\ \tau^e(\theta) &= \frac{2G \cdot n^2 \cdot \cos\theta}{2G \cdot n^2 \cdot \cos\theta \cdot \cos\phi + i \cdot \sin\phi \cdot (G^2 + n^4 \cdot \cos^2\theta)}. \end{aligned} \quad (48)$$

The reflection coefficients for the propagating waves are

$$\begin{aligned} \rho^m_{\text{prop}}(\theta) &= \frac{i \cdot \sin\phi \cdot \left(\cos^2\theta - G^2\right)}{2G \cdot \cos\theta \cdot \cos\phi + i \cdot \sin\phi \cdot (G^2 + \cos^2\theta)}; \\ \rho^e_{\text{prop}}(\theta) &= \frac{i \cdot \sin\phi \cdot \left(G^2 - n^4 \cdot \cos^2\theta\right)}{2G \cdot n^2 \cdot \cos\theta \cdot \cos\phi + i \cdot \sin\phi \cdot (G^2 + n^4 \cdot \cos^2\theta)}. \end{aligned} \quad (49)$$

The reflection coefficients for evanescent waves, characterized by imaginary angles, can be found using the formulas

$$\begin{aligned} \rho^m_{\text{evan}}(\theta) &= \frac{y - \gamma_n}{y + \gamma_n} \cdot \frac{1 - \exp(-2Q_y)}{1 - \exp(-2Q_y) \cdot \left(\dfrac{y - \gamma_n}{y + \gamma_n}\right)^2}; \\ \rho^e_{\text{evan}}(\theta) &= \frac{-n^2 y + \gamma_n}{n^2 y + \gamma_n} \cdot \frac{1 - \exp(-2Q_y)}{1 - \exp(-2Q_y) \cdot \left(\dfrac{n^2 y - \gamma_n}{n^2 y + \gamma_n}\right)^2}. \end{aligned} \quad (50)$$

3. RESULTS OF COMPUTATIONS FOR A PARALLEL-PLANE CASE

Mere study of power fluxes in the proximity of a layer (or layers) of absorbing dielectric materials is not of special interest, because it is difficult to practically measure power fluxes, and especially to separate contributions of propagating and evanescent modes. It is much more practical and useful to study the radiation and absorption efficiencies of radiators near dielectric layers, including those used for shielding purposes. The algorithm represented in Section 2 allows for calculating these efficiencies for the elementary electric and magnetic dipoles near dielectric layers. In the present Section, some computational results are represented for composite absorbing materials, containing conductive inclusions. The materials considered herein are of two types: (1)

composite dielectrics (when concentration of conducting inclusions in the dielectric base is below the percolation threshold), and (2) poor conductors (when concentration of inclusions is high enough to form a conducting path).

Example 1. The horizontal magnetic and electric dipoles are placed at the height h above the boundary of two lossy dielectric media, as shown in Figure 5.

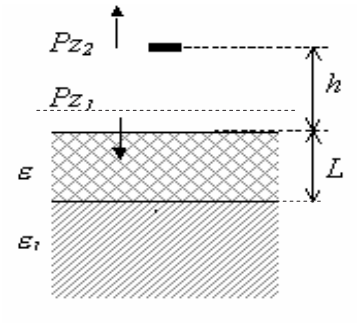

Figure 5. Two-layered parallel-plane structure.

The dielectric layer having the relative dielectric constant ε and finite thickness L (upper layer) is placed upon the semi-infinite layer with the relative dielectric constant ε_1 (lower medium). The surrounding medium (above the dielectric media) is air. The total radiated power is determined by two fluxes P_{z1} and P_{z2}, calculated according to the formulas in Section 2. The power flowing through the cross-section Z_1 contains two components: (1) the power transmitted by the propagating waves at $|\chi| < k_0$ (17), and (2) the power transmitted by the evanescent (inhomogeneous) waves determined by the near fields at $|\chi| \geq k_0$ (18). The effect of evanescent waves becomes noticeable, when the source is placed closer to the boundary, or when the ratio of the height to the wavelength (h/λ) decreases. This is related to the effect of an increase of the near-field penetration into a lossy dielectric. The dependence of the normalized power flux as a function of the parameter h/λ, is shown in Figure 6. The power flux of the propagating wave is independent on h, and is normalized to be a unity.

Radiation efficiency η_{rad} (in dimensionless units) of the electric or magnetic elementary dipoles versus h/λ for various parameters of the dielectric layers is shown in Figures 7(a), (b) and 8(a), (b). Dielectrics in this example are lossy, but their permittivity is assumed to be frequency-independent in the frequency range of interest. The lower medium is moist soil (Figures 7) or dry wood (Figures 8), and

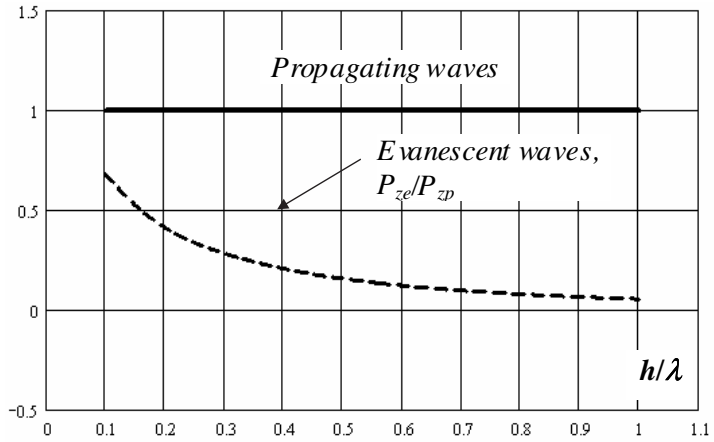

Figure 6. Normalized power of propagating and evanescent waves. The lower dielectric layer is the moist soil, $\varepsilon_1 = 8.0 - i0.5$. The upper layer is of the thickness $L = 0.35\lambda$, $\varepsilon = 1.6 - i0.1$ (porous material).

the dielectric parameters of the upper finite-thickness layer are taken different — for a porous material, for dry wood, and for concrete or brick. As seen from the graphs in Figures 7 and 8, the radiation efficiency of a dipole abruptly decreases, when the source is placed close to the absorbing layer. This can be explained by the increase of power flux due to the evanescent waves.

Example 2. Figures 9(a), (b) and 10(a), (b) show the dependences of the absorption efficiency (in dimensionless units) for electric and magnetic dipoles placed parallel to the layer of the thickness L versus relative height h/λ. The layer in this example is surrounded by air ($\varepsilon_1 = 1$). The graphs are calculated for different values of complex permittivity of the layer in Figures 9, and for different values of relative thickness L/λ in Figure 10. As seen from the graphs, the absorption efficiency increases as the near-field interaction with the dielectric increases. The near fields are determined by the evanescent waves, and the latter are more intense at the shorter distances from the radiator. Thus, when the radiator is placed closer to the absorbing medium ($h/\lambda \to 0$), loss increases because of the substantial increase of near fields. However, the behavior of the graphs in Figures 9 and 10 depend on the particular values of permittivity and the thickness of the dielectric layer. Since at some values of (h/λ) and permittivity ε a layer might have a resonance thickness ($\sim \frac{\lambda}{2\sqrt{\varepsilon}}$), the behavior of the curves for different permittivities with respect to (h/λ)

might differ.

Example 3. Consider the behavior of the near-field of an elementary electric dipole close to a planar composite dielectric layer with a frequency-dispersive permittivity. A composite material is an

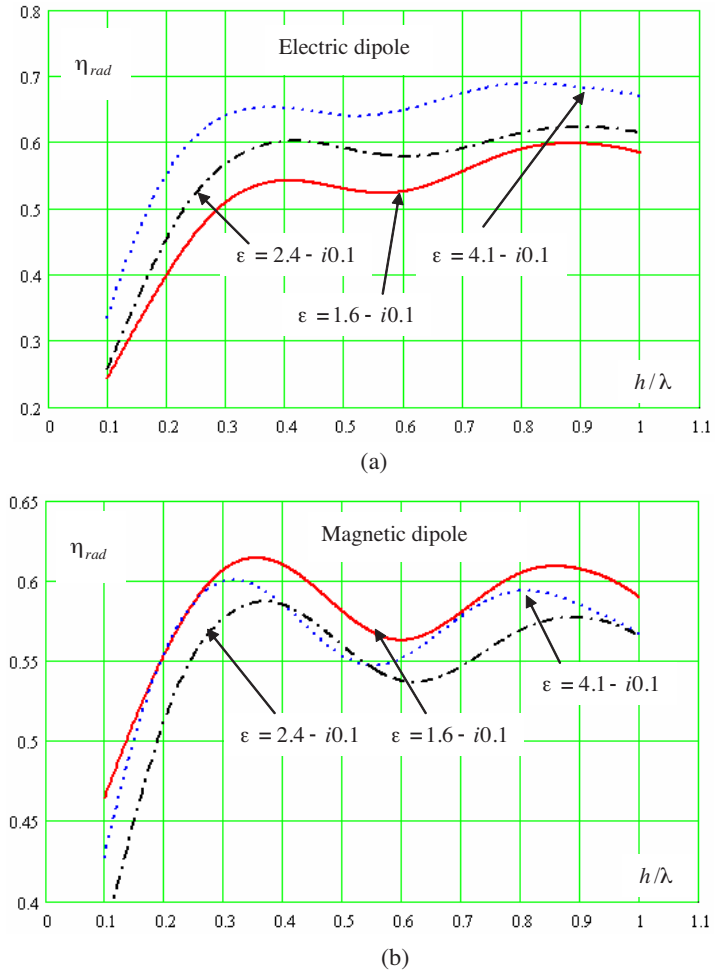

Figure 7. Radiation efficiency of (a) an electric dipole; (b) a magnetic dipole. The geometry is as in Figure 5 (radiation of an antenna above the surface). The lower dielectric layer is the moist soil, $\varepsilon_1 = 8.0 - i0.5$. The upper layer is of the thickness $L = 0.35\lambda$. The solid line corresponds to the porous material; the dash-dot line corresponds to dry wood, and the dotted line is for brick or concrete.

inhomogeneous medium. However, its electromagnetic parameters may be homogenized using an effective medium theory (EMT). There are many effective media theories (EMT) allowing for homogenization of composite media [19–23]. This layer contains conductive fibers in

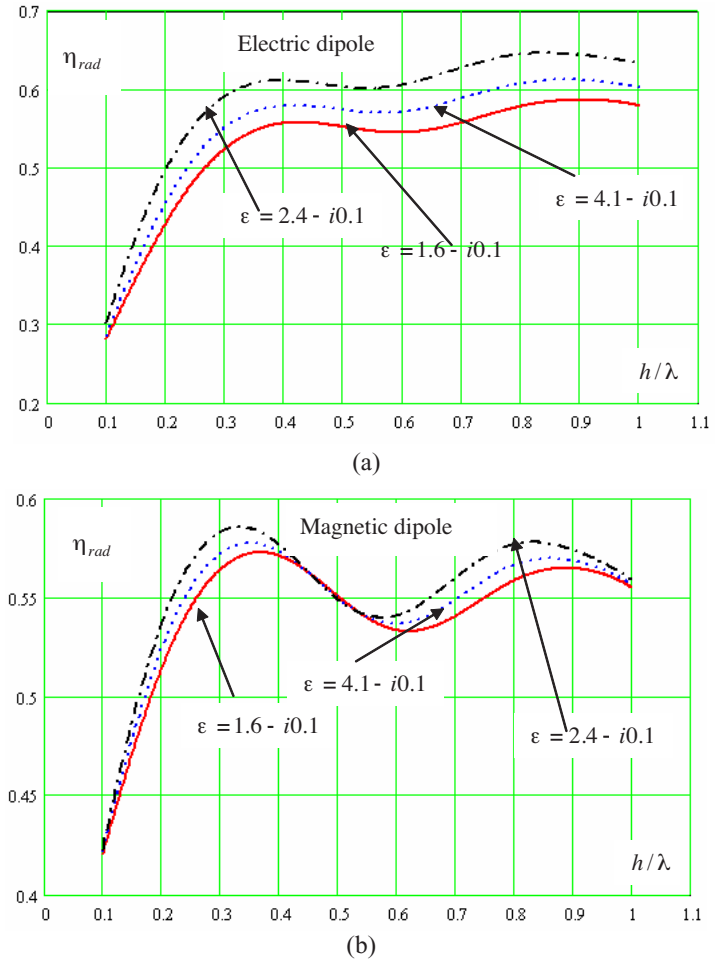

Figure 8. Radiation efficiency of (a) an electric dipole; (b) a magnetic dipole. The geometry is as in Figure 5 (radiation of an antenna above the surface). The lower dielectric layer is the dry wood, $\varepsilon_1 = 2.4 - i0.5$. The upper layer is of the thickness $L = 0.35\lambda$. The solid line corresponds to the porous material; the dash-dot line corresponds to dry wood, and the dotted line is for brick or concrete.

the dielectric base. The frequency characteristics for the permittivity of the composite are calculated using the Maxwell Garnett effective medium formulation [24–31], described in *Appendix C*, and they are shown in Figures 11(a), (b). The base dielectric is assumed to be non-dispersive ($\varepsilon_b = 2.2$). Aspect ratio for fibers (ratio of their length to their diameter) is $a = 1500$, and their volumetric fraction in the base material is 0.15%. The dependences of the absorption coefficient versus distance of the electric dipole from the

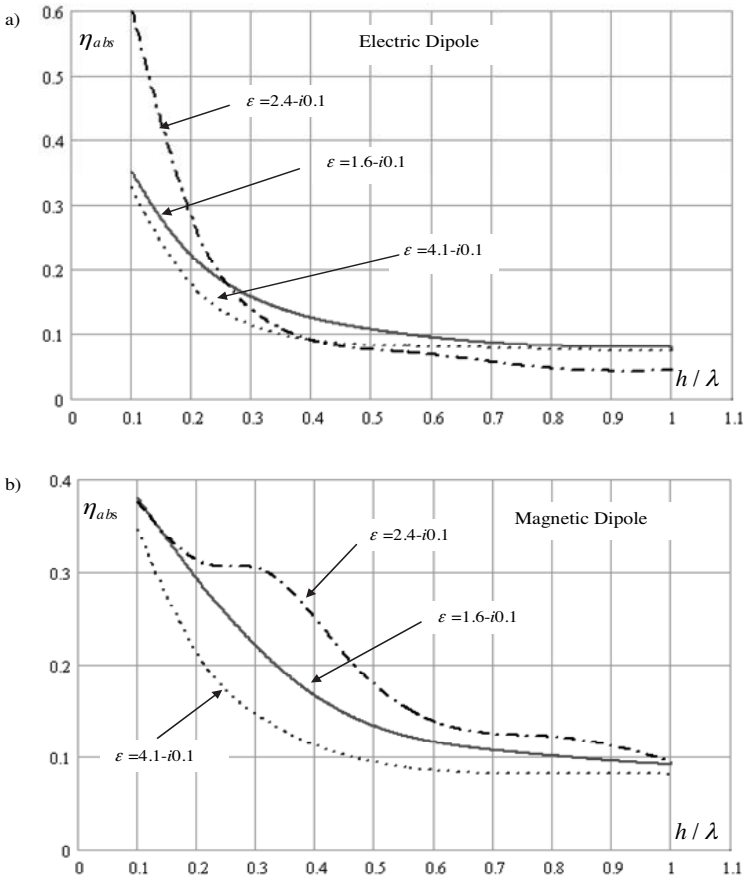

Figure 9. Absorption efficiency for (a) an electric dipole; (b) a magnetic dipole. The geometry is as in Figure 1 (heating of a dielectric layer of a finite thickness). The dielectric layer is of the thickness $L = 0.35\lambda$. The solid line is for porous material; the dash-dot line is for dry wood, and the dotted line is for brick or concrete.

composite layer for different frequencies are shown in Figures 12(a)–(e). Conductivity of inclusions is a varying parameter. When the point of observation is in the far-field region (see graphs for 9 GHz), the absorption increases (the calculated value $\eta_{\mathrm{abs,dB}} = 10\log_{10}(\eta_{\mathrm{abs}})$ becomes closer to 0 dB) with the increase of conductivity of inclusions. This result is obvious: the higher conductivity of fibers leads to the increase of polarizability of inclusions, and to the increase of static dielectric susceptibility, and, according to the Kramers-Kronig causality relations, increase of the imaginary part of the permittivity at

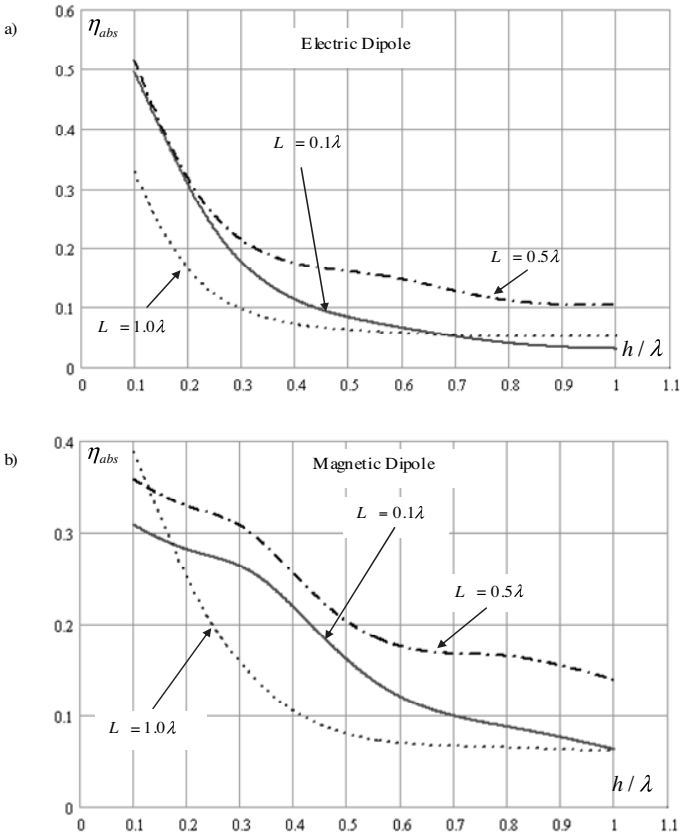

Figure 10. Absorption efficiency of (a) an electric dipole; (b) a magnetic dipole. The geometry is as in Figure 1 (heating of a dielectric layer of a finite thickness). The dielectric layer is the dry wood, $\varepsilon = 2.4 - i0.1$. The solid line corresponds to the layer thickness 0.1λ; the dash-dot line is for 0.5λ, and the dotted line is for 1.0λ.

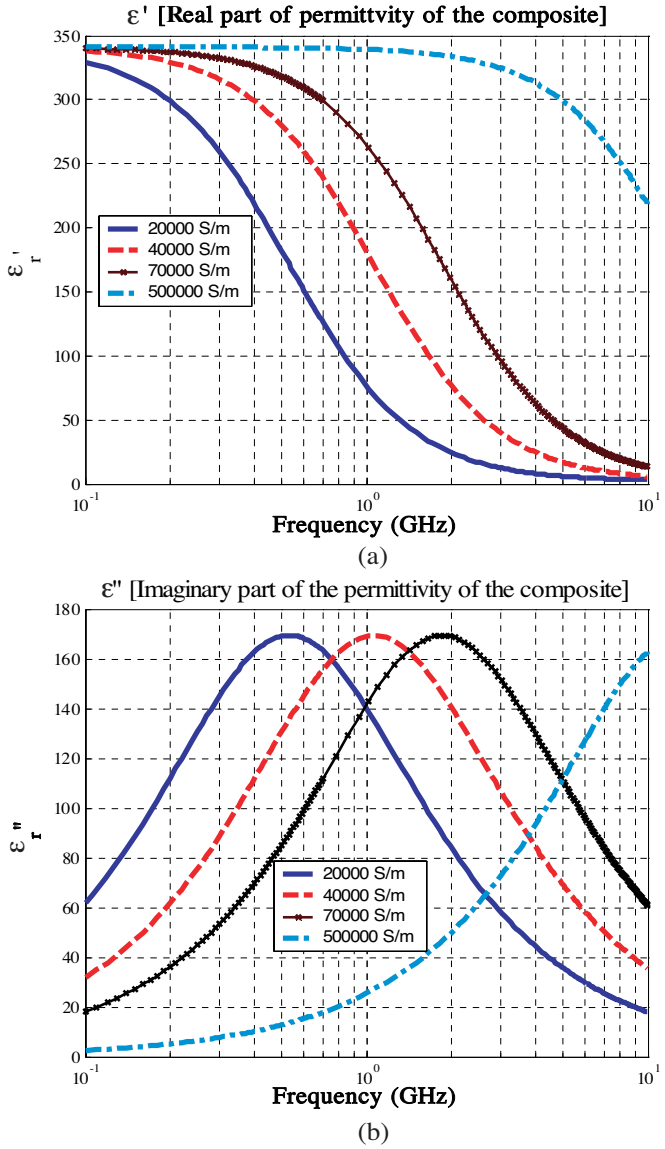

Figure 11. Complex permittivity of the composite (a) real part; (b) imaginary part of permittivity. Permittivity of the base material is $\varepsilon_b = 2.2$; parameters of fibers: aspect ratio $a = 1500$, volumetric fraction is $f_i = 0.15\%$, and conductivity is a varying parameter.

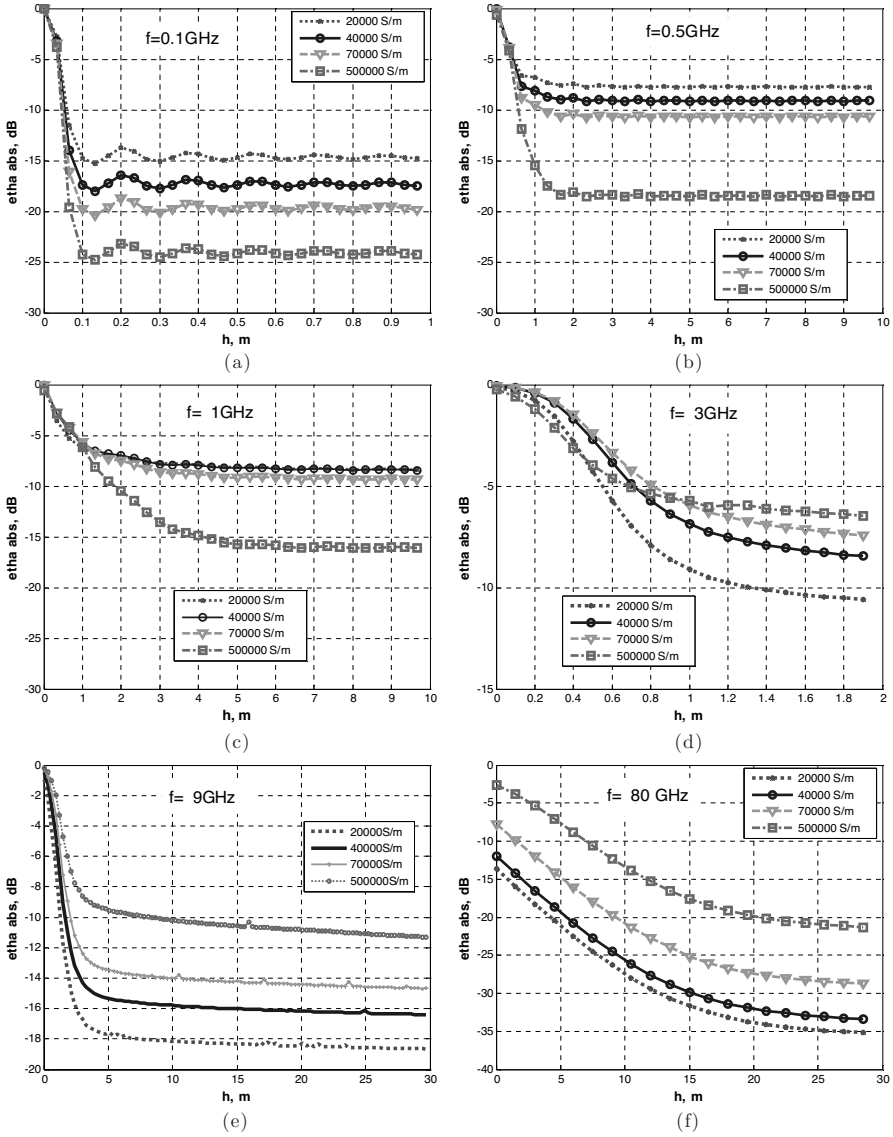

Figure 12. Absorption efficiency (dB) versus distance between the electric dipole and the composite layer ($L = 1\,\text{mm}$); frequency is (a) 0.1 GHz, (b) 0.5 GHz, (c) 1 GHz, (d) 3 GHz, (e) 9 GHz, and (f) 80 GHz. Aspect ratio of fibers is 1500. Conductivity σ of fibers is a parameter.

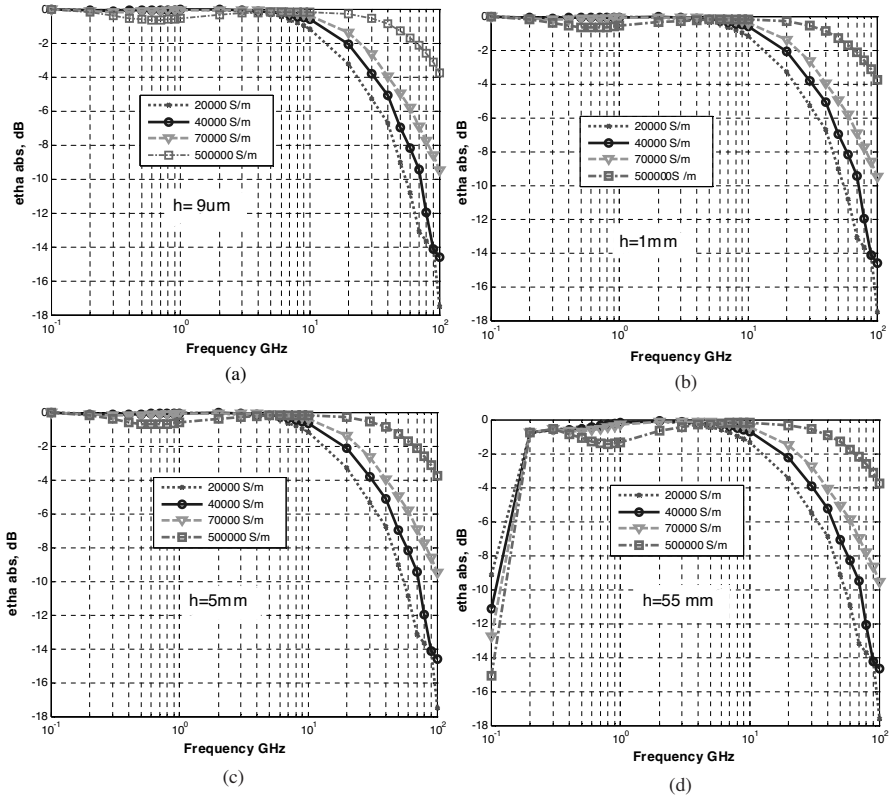

Figure 13. Absorption efficiency (dB) versus frequency for the electric dipole and the composite layer of thickness L=1 mm for different distances from the source (a) $h = 9\,\mu$m; (b) $h = 1\,$mm, (c) $h = 5\,$mm; (d) $h = 55\,$mm. Aspect ratio is 1500. Conductivity of fibers is a parameter.

the frequency of maximum loss. However, in the near-field region the higher conductivity does not necessarily lead to the higher absorption. When the electric source is close to the composite layer (near-fields at 0.1 and 0.5 GHz), the situation is the opposite: the higher the conductivity of inclusions, the lower the absorption efficiency becomes. This might be explained by the fact that the concept of effective permittivity is valid only for the far-field region in principle, and for the near-field region local interactions through inhomogeneous fields, including evanescent modes, should be taken into account when estimating effective permittivity.

Figures 13(a), (b) show the absorption efficiency (dB) versus

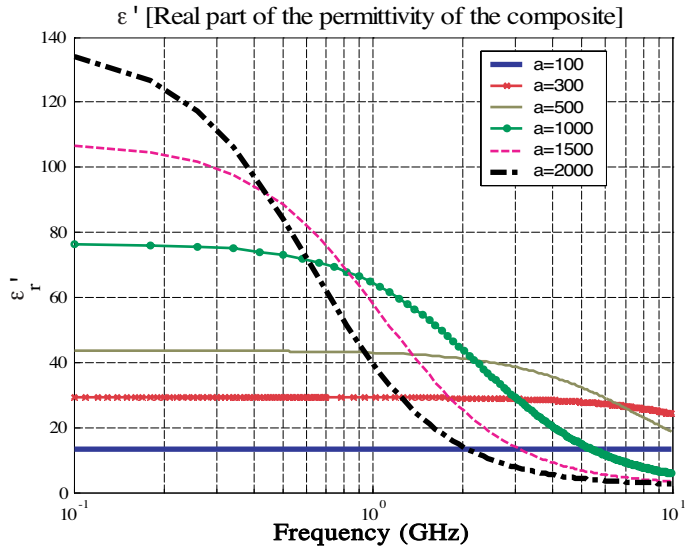

(a)

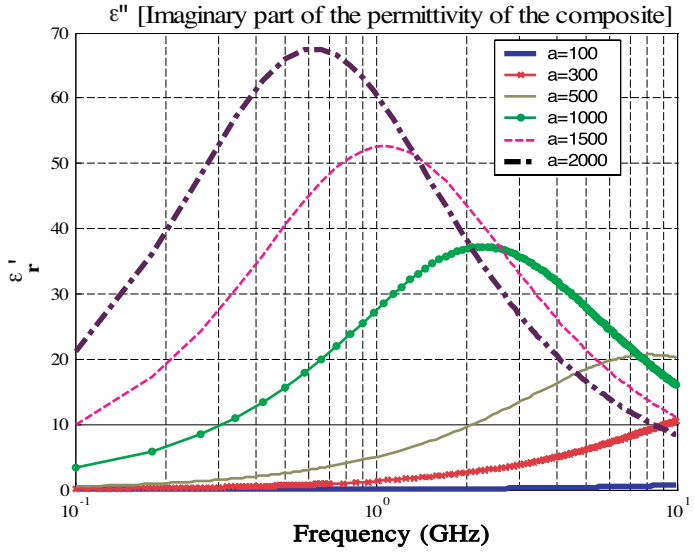

(b)

Figure 14. Complex permittivity of the composite: (a) real part; (b) imaginary part. Base material is Teflon ($\varepsilon' = 2.2$); volumetric fraction of carbon inclusions is $0.7/a < p_c$; conductivity is $\sigma = 40000\,\mathrm{S/m}^2$; aspect ratio is a varying parameter.

frequency for the electric dipole and the composite layer ($L = 1\,\text{mm}$) at different distances from the source: $h = 1\,\text{mm}$ and $h = 5\,\text{mm}$, when the conductivity of inclusions is different. As seen from the graphs, at higher conductivity and smaller distance of the layer from the source, the "resonance" behavior of the absorption efficiency versus frequency is more pronounced. At some frequencies (in a comparatively low frequency range) the layer becomes less absorbing with the increase of conductivity. The "resonance" frequency of minimal absorption shifts to the higher frequencies with the increase of conductivity, as shown in Figures 11(a), (b).

Example 4. Another set of graphs is obtained for the similar composite as in Example 3, but the aspect ratio of inclusions (ratio of the length to the diameter) is a varying parameter. The composite

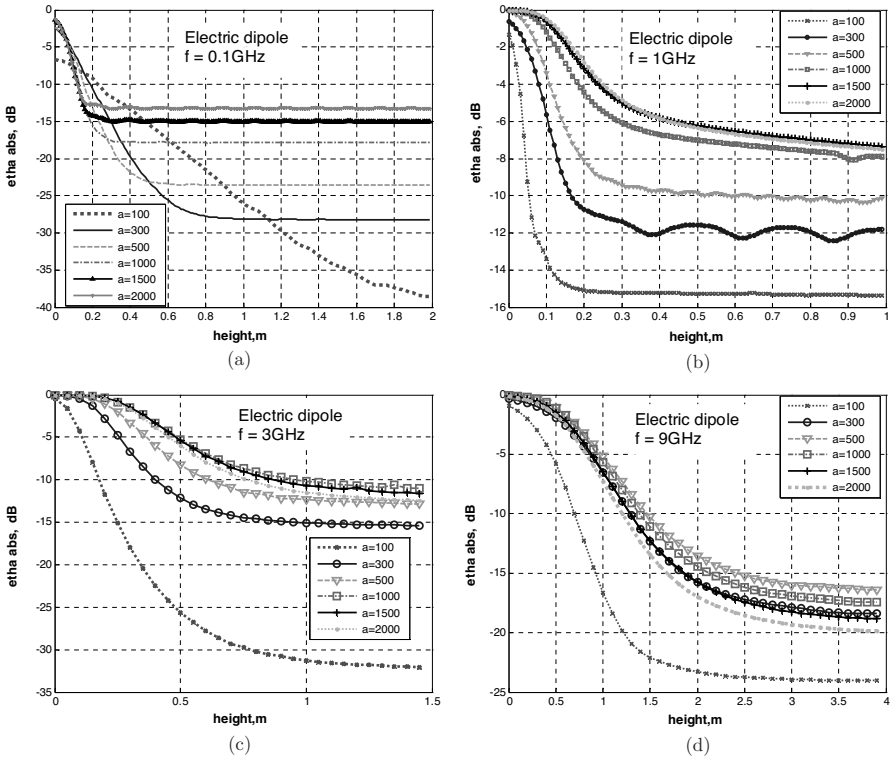

Figure 15. Absorption coefficient versus distance h between the elementary electric dipole and the composite layer (thickness $L = 1\,\text{mm}$); frequency is (a) 0.1 GHz, (b) 1 GHz, (c) 3 GHz, and (d) 9 GHz. Aspect ratio a of inclusions is a parameter.

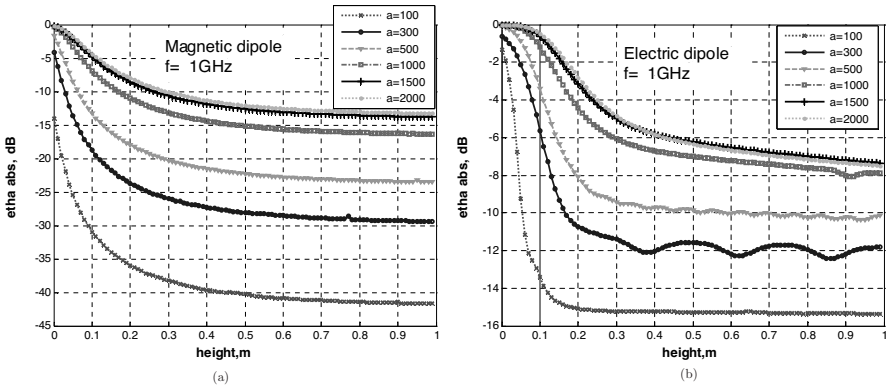

Figure 16. Absorption coefficient versus distance h between the composite layer and (a) elementary magnetic dipole, and (b) elementary electric dipole. Thickness of the layer is $L = 1\,\text{mm}$.

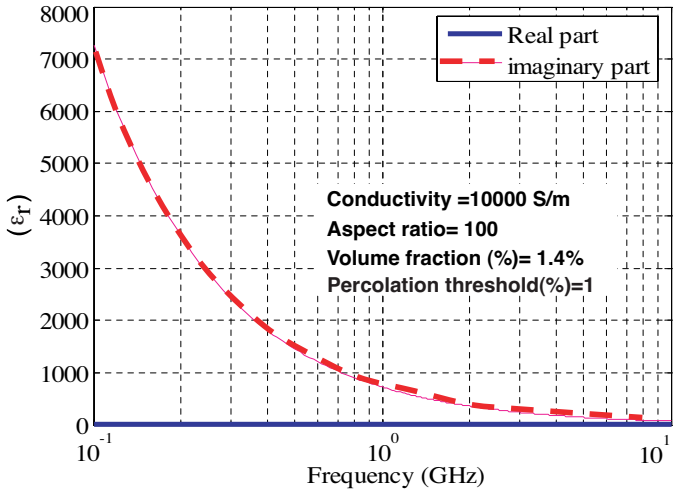

Figure 17. Relative permittivity of a conducting composite layer (volume fraction of conducting inclusions is above the percolation threshold).

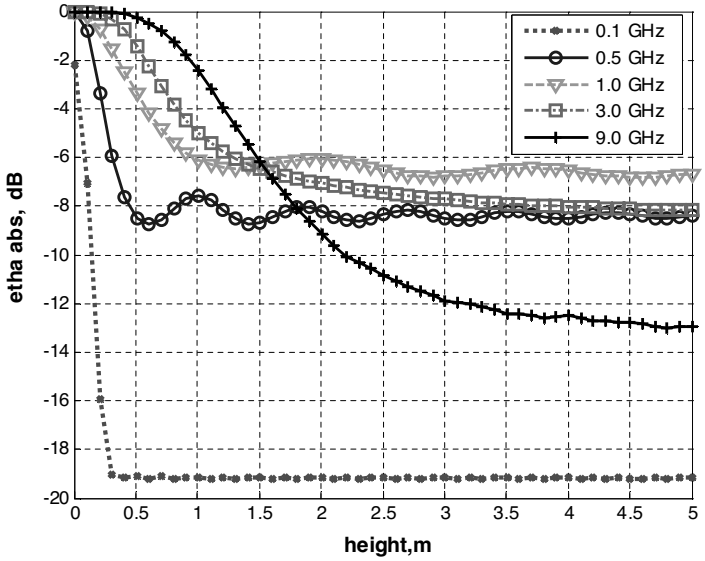

Figure 18. Absorption efficiency as a function of height for an elementary electric dipole placed near the conducting composite layer with frequency characteristic shown in Figure 17. Thickness of the layer is $L = 1\,\text{mm}$.

is still a dielectric with concentration of conducting fibers much smaller than the percolation threshold. The frequency dependences of the real and imaginary parts of effective permittivity are shown in Figure 14(a), (b). Figures 15(a)–(d) contain the graphs for the absorption efficiency η_{abs} versus distance h between the elementary electric dipole and the composite layer (thickness $L = 1\,\text{mm}$) for different frequencies. As seen from Figures 15, the absorption efficiency of near fields does not necessarily increase with the increase of the fiber aspect ratio. Figures 16(a), (b) show the absorption efficiency as a function of the distance h between the composite layer and the elementary magnetic dipole, and the composite layer and the elementary electric dipole. Absorption efficiency in a dielectric composite for an elementary magnetic dipole is smaller than that for an elementary electric dipole.

The results of computations for near-field of an elementary electric dipole close to a plane composite layer show that the behavior of absorption of near fields in the composite layer with respect to the conductivity and aspect ratio of inclusions is different from the far-field behavior. Near-field absorption in a layer depends on the distance

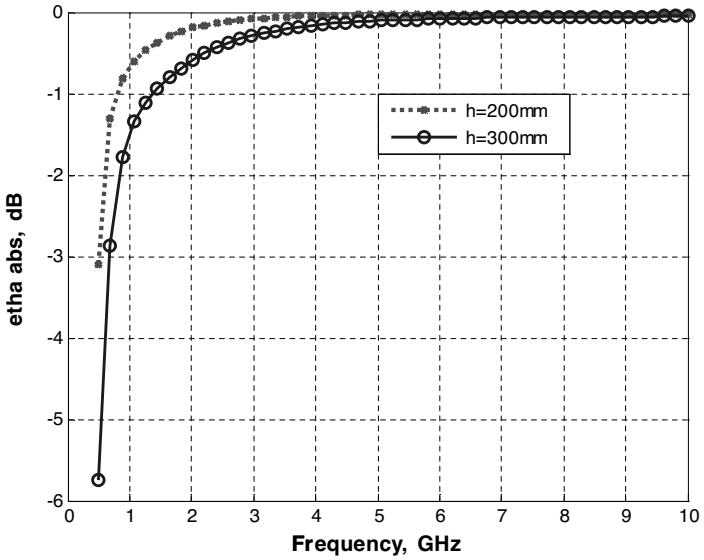

Figure 19. Absorption efficiency for an elementary electric dipole close to the composite conducting layer with frequency characteristic shown in Figure 17. Thickness of the layer is 1 mm.

of the radiator from the composite layer and the particular effective permittivity of the composite layer at the particular frequency.

Example 5. The behavior of elementary radiators has been also studied in proximity of a composite layer with a concentration of conducting fibers above the percolation threshold, so that this composite is a poor dielectric and a poor conductor. This composite contains conducting inclusions at a concentration above the percolation threshold. The composites with high concentration of inclusions are described, for example, by McLachlan [32] or Ghosh-Fuchs approximations [33]. The complex permittivity of the composite was calculated using McLachlan's approximation [32, 34], represented also in *Appendix C.* Since this is a conducting composite, the imaginary part of its permittivity increases with the decrease of frequency as $1/\omega$, and is much greater than the real part. The frequency dependence for permittivity of the composite is shown in Figure 17. Figure 18 represents the absorption efficiency as a function of height for an elementary electric dipole placed near the conducting composite layer with the frequency characteristic shown in Figure 17.

Different curves in Figure 18 correspond to different frequencies (0.1–9 GHz). Figure 19 shows the frequency behavior of absorption

efficiency, when the electric dipole is placed at the heights 200 and 300 mm above the conducting layer. The absorption efficiency of a radiator close to the composite conducting layer depends on the distance between the radiator and frequency behavior of the imaginary part of the permittivity of the layer.

These examples show that the near-field and far-field behavior of radiators in the proximity of dielectric and conducting composite layers might be substantially different. One of the possible explanations of this phenomenon is that the effective medium theories used for homogenization to obtain effective constitutive parameters of media are suitable only for far-field considerations, since they do not take into account near-field interactions. Anyway, physical reasons still need to be studied, and the presented method is a convenient tool for this.

4. CONCLUSIONS

In this paper, it is shown that the behavior of electric and magnetic radiators in proximity of planar layered dielectric structures containing layers of composite dielectrics with engineered frequency responses can be modeled using the rigorous analytical Unified Spectral Approach (UST). Herein, the UST, which is a general formulation valid for any canonical geometry, has been specified for a particular case - planar layered dielectric structures. The formulation allows for calculating power fluxes of sources of any type and complexity. An important advantage of the method is that the power fluxes are represented in an explicit form via their spectra, avoiding cumbersome calculations via field components. The formulation is useful for evaluating power loss in multilayered structures, when they are in the near-field region of the source.

The formulas obtained for the power fluxes are original and take into account the influence of dielectric layers of different geometry on the field structure. The presented approach is a reasonable addition to the eigenfunctions technique, and it is useful for the solution of a wide range of theoretical and applied electromagnetic problems.

The represented rigorous analytical approach has been used to characterize the near-field behavior of elementary electric and magnetic dipoles close to a plane layer (or layers) of engineered composite materials. Some computational results are obtained for composite media containing conductive inclusions. These composites provide shielding mainly due to absorption of electromagnetic energy. The effect of conductivity of inclusions and their geometry (through their aspect ratio) on the absorption and radiation efficiency of a radiator near composite layers is analyzed. The computational results for the

near-field of an elementary electric dipole close to a plane composite layer show that the behavior of the absorption of the near fields in the composite layer with respect to the conductivity and aspect ratio of inclusions is different from the far-field behavior. Near-field absorption in a layer depends on the distance of the radiator from the composite layer and the particular effective permittivity of the composite layer at the particular frequency.

APPENDIX A. CALCULATION OF THE POWER FLUX IN THE CYLINDRICAL LAYERED STRUCTURE

In the cylindrical case shown in Figure 2, the radial component of the Poynting vector is

$$p_r = 0.5 \cdot \mathrm{Re}\left(E_\varphi H_z^* - E_z H_\varphi^*\right). \tag{A1}$$

The E- and H-field components in (A1) can be represented as the Fourier integral along the z-coordinate, and expanded as the Fourier series along the φ-coordinate, as proposed in [11]. Then the application of the Plancherel's theorem yields simplification, since a product of two complex-conjugated functions in the integrand is substituted as the product of their Fourier transforms [12]. The power flux P_r is found from (5) as

$$P_r = 2\pi^2 \mathrm{Re} \sum_n \int_\chi \left(e_{\varphi n} h_{zn}^* - e_{zn} h_{\varphi n}^*\right) r d\chi, \tag{A2}$$

the electric spectrum densities $e_{\varphi n}$ and e_{zn}, as well as the magnetic field spectrum densities $h_{\varphi n}$ and h_{zn} are used. Similar to (11) for a parallel-plane case, the spectrum densities $e_{\varphi n}$, e_{zn}, $h_{\varphi n}$, and h_{zn} appear to be the scalar potentials.

Substitution of the Fourier representations for all the field and current components into Maxwell's equations results in the Bessel differential equations for e_{zn} and h_{zn} spectrum densities [11, 12]. Taking into account the relation between the field spectrum components [11, 12], the spectrum densities $e_{\varphi n}$ and $h_{\varphi n}$ can be expressed in terms of the spectrum densities e_{zn} and h_{zn}:

$$\begin{aligned} e_{\varphi n} &= \frac{1}{\gamma^2}\left(-\frac{\chi n}{r} e_{zn} + i\omega\mu \frac{\partial h_{zn}}{\partial r}\right); \\ h_{\varphi n} &= \frac{1}{\gamma^2}\left(-\frac{\chi n}{r} h_{zn} - i\omega\varepsilon \frac{\partial e_{zn}}{\partial r}\right). \end{aligned} \tag{A3}$$

Then (A2) can be represented as

$$P_r = 2\pi^2 \sum_n \int_\chi \frac{ik}{\gamma} \left(Z \frac{dh_{zn}}{dr} h^*_{zn} - \frac{1}{Z} \frac{de_{zn}}{dr} e^*_{zn} \right) r d\chi, \qquad \text{(A4)}$$

where the propagation constant is $\gamma^2 = k^2 - \chi^2$, and $Z = \sqrt{\mu/\varepsilon}$ is the characteristic impedance of the medium, and $k = \omega\sqrt{\varepsilon\mu}$.

The solution of the mentioned above Bessel differential equation for e_{zn} and h_{zn} inside the cylindrical structure is the following [11]

$$\begin{aligned} h_{zn} &= J_{in} H_n^{(2)}(\gamma \cdot r) + J_r H_n^{(1)}(\gamma \cdot r); \\ e_{zn} &= U_{in} H_n^{(2)}(\gamma \cdot r) + U_r H_n^{(1)}(\gamma \cdot r). \end{aligned} \qquad \text{(A5)}$$

It should be mentioned that the coefficients $J_{in,r}$ and $U_{in,r}$ in (A5) are known from the solution of the boundary problem, and they are independent of the coordinate r. These coefficients are analogous to the generalized "currents" and "voltages" in (15). $H_n^{(1),(2)}(\gamma \cdot r)$ are the I and II type Hankel functions, respectively.

Two cases should be considered: (1) $|\chi| < k$, and (2) $|\chi| \geq k$.

(1) When $|\chi| < k$, the propagation constant γ is real. Then, substituting (A5) in (14), the power flux can be obtained,

$$P_r = 4\pi^2 k \sum_n \int_\chi \frac{1}{\gamma^2} \left(Z \left(|J_{in}|^2 - |J_r|^2 \right) + \frac{1}{Z} \left(|U_{in}|^2 - |U_r|^2 \right) \right) d\chi. \qquad \text{(A6)}$$

(2) When $|\chi| > k$, the propagation constant $\gamma = -i\beta$ is imaginary. Since the argument of the Hankel functions becomes imaginary, they transform into the modified Bessel functions K_n and I_n. Then the solutions of the differential equation for the spectra e_{zn} and h_{zn} are

$$\begin{aligned} h_{zn} &= 2(i)^n \left(\frac{i}{\pi} (J_{in} - J_r) K_n(\gamma \cdot r) + (-1)^n J_r I_n(\gamma \cdot r) \right); \\ e_{zn} &= 2(i)^n \left(\frac{i}{\pi} (U_{in} - U_r) K_n(\gamma \cdot r) + (-1)^n U_r I_n(\gamma \cdot r) \right). \end{aligned} \qquad \text{(A7)}$$

Substituting the solutions (A7) in (A2) and using some algebraic manipulations, one can get

$$P_r = 8\pi \sum_n \int_\chi (-1)^n \frac{k}{\gamma^2} \left(Z R_{Hn} + \frac{1}{Z} R_{En} \right) d\chi, \qquad \text{(A8)}$$

where

$$\begin{aligned} R_{En} &= \mathrm{Re}\left[U_r^*\left(U_{in}-U_r\right)\right]; \\ R_{Hn} &= \mathrm{Re}\left[J_r^*\left(J_{in}-J_r\right)\right]. \end{aligned} \tag{A9}$$

The coefficients (A9) have the physical meaning of the radiation resistance for the fields of E- and H-types, respectively. The power flux (A8) through the surface crossing the medium without losses is independent of the coordinate r. Similarly to the case of a parallel-plane layered structure, the power flux in the semi-infinite region is determined by the propagating and evanescent waves.

APPENDIX B. CALCULATION OF THE POWER FLUX IN A SPHERICAL LAYERED STRUCTURE

An electromagnetic power flux through the sphere of the radius R shown in Figure 3, can be found from (5), taking into account the R-component of the Poynting vector,

$$p_R = 0.5 \cdot \mathrm{Re}\left(E_\theta H_\varphi^* - E_\varphi H_\theta^*\right). \tag{B1}$$

The scalar potentials of electric and magnetic types can be introduced analogously to the scalar potential $\Phi^{e,m}$ and $\Psi^{e,m}$ for the parallel-plane layered structure [13]. These scalar potentials can be expanded as a series of eigenfunctions for the Laplace operator, and the tangential field components can be represented as

$$\begin{aligned} \vec{E}_\tau &= \frac{1}{R}\left(\sum_{n,m} U_{nm}^e \vec{t}_{nm} + \sum_{n,m} U_{nm}^m \vec{\tau}_{nm}\right); \\ \vec{H}_\tau &= \frac{1}{R}\left(\sum_{n,m} I_{nm}^m \vec{t}_{nm} - \sum_{n,m} I_{nm}^e \vec{\tau}_{nm}\right), \end{aligned} \tag{B2}$$

where $I_{nm}^{e,m}$ are the spectra of the potential $\Phi^{e,m}$, and $U_{nm}^{e,m}$ are the spectra of the potential $\Psi^{e,m}$. Vectors $\vec{t}_{nm}$ and $\vec{\tau}_{nm}$ in (B2) represent the complete orthogonal system of vector functions, so that

$$\begin{aligned} \vec{t}_{nm} &= \frac{dT_{nm}}{d\theta}\vec{\theta}_o + \frac{1}{\sin\theta}\frac{dT_{nm}}{d\varphi}\vec{\varphi}_o; \\ \vec{\tau}_{nm} &= \frac{1}{\sin\theta}\frac{dT_{nm}}{d\varphi}\vec{\theta}_o - \frac{dT_{nm}}{d\theta}\vec{\varphi}_o, \end{aligned} \tag{B3}$$

where $T_{nm} = P_n^m(\cos\theta)\cdot e^{jm\varphi}$ is the I type Legendre function [15], and $\vec{\theta}_o$ and $\vec{\varphi}_o$ are the unit orthogonal vectors in spherical coordinate

system. Orthogonality of the vector functions $\vec{t}_{nm}$ and $\vec{\tau}_{nm}$ is proved using the formula (20) in [15, Section 7.12]. Substitution of the orthogonal vector functions (B3) in (B2) and then in (B1), yields the following expression for the power flux,

$$P_R = 2\pi \mathrm{Re} \sum_{nm} iQ_{nm} \left(Z \frac{dJ^e_{nm}}{d\rho} J^{e*}_{nm} - \frac{1}{Z} \frac{dU^{m*}_{nm}}{d\rho} U^m_{nm} \right), \tag{B4}$$

where the distance $\rho = kR$, k is a wave number, Z is the characteristic impedance of the medium, and the coefficients Q_{nm} are

$$Q_{nm} = \frac{n(n-1)(n+m)!}{(2n+1)(n-m)!}. \tag{B5}$$

Consider the area where the reflected wave exists in the spherical case shown in Figure 3. The solution of the differential equation for the generalized currents and voltages in this case can be represented as

$$\begin{aligned} U^m_{nm} &= \tilde{U}_{in} \xi_n(\rho) + \tilde{U}_r \eta(\rho); \\ J^e_{nm} &= \tilde{J}_{in} \xi_n(\rho) + \tilde{J}_r \eta(\rho), \end{aligned} \tag{B6}$$

where

$$\begin{aligned} \xi_n(\rho) &= \sqrt{\frac{\pi \cdot \rho}{2}} \cdot H^{(2)}_{n+1/2}(\rho); \\ \eta_n(\rho) &= \sqrt{\frac{\pi \cdot \rho}{2}} \cdot H^{(1)}_{n+1/2}(\rho). \end{aligned} \tag{B7}$$

In (B7), $H^{(1)}_{n+1/2}(\rho)$, $H^{(2)}_{n+1/2}(\rho)$ are the type I and II Hankel functions, respectively. The amplitudes $\tilde{U}_{in,r}$ and $\tilde{J}_{in,r}$ are found from the solution of the corresponding boundary problem for the fields E_τ, H_τ. If there are no reflected waves in a region, the amplitudes $\tilde{U}_r$ and $\tilde{J}_r$ are zero.

Substituting (B6) in (B1), one can get

$$P_R = 2\pi \sum_{nm} Q_{nm} \left(Z \left| \tilde{J}_{in} \right|^2 + \frac{1}{Z} \left| \tilde{U}_{in} \right|^2 - Z \left| \tilde{J}_r \right|^2 - \frac{1}{Z} \left| \tilde{U}_r \right|^2 \right), \tag{B8}$$

As follows from (B8), the transferred energy is independent of the distance R in the medium without losses, similar to the parallel-plane and cylindrical layered geometries. However, in the spherical case, in contrast to the parallel-plane and cylindrical cases, all the eigenwaves are propagating. The reason for this is that in the structure of the

solution for the spherical geometry there are no evanescent waves. The functions $\xi_n(\rho)$ and $\eta_n(\rho)$ at large ρ have an asymptotic $e^{-i\rho}$, $e^{i\rho}$ at any n, and they describe propagating waves. In the planar and cylindrical geometries, in contrast with the spherical case, at large spectral parameters the corresponding functions describe evanescent waves. This is a mathematical fact, and its physical interpretation is not quite evident.

APPENDIX C. MODELS OF DIELECTRIC AND CONDUCTING COMPOSITE MEDIA

There are many effective media theories (EMT) allowing for homogenization of composite media [19–23], that is, characterization of composites by effective permittivity and permeability. To find effective electromagnetic properties of composite media, it is important to know the electromagnetic parameters of a base (host matrix) material and inclusions. A composite material containing conducting inclusions in a dielectric base has frequency-dependent effective permittivity.

The base material might be quite transparent over the frequency range of interest. However, if there are conducting inclusions, the electromagnetic energy may be absorbed due to conductivity loss and to the dimensional resonance in the inclusions. Presence of conductive particles will also increase reflection from the composite layer. If a composite contains a dilute phase of conducting inclusions, it remains a dielectric material. If the concentration of conducting inclusions is high, above the percolation threshold, the material is a conductor. Percolation threshold in the conductor-insulator composite materials is defined as the concentration of the conductive filaments, where the electrical properties of the composite changes drastically from insulator to conductor. The mechanism of interaction with electromagnetic waves incident on a conducting composite is mainly reflection.

The Maxwell Garnett (MG) model [24–27] is the simplest and the most widely used for description of composite media at comparatively low concentrations of inclusions. Its important feature is linearity with respect to frequency and applicability for a multiphase mixture. The generalized MG mixing formula for multiphase mixtures with randomly

oriented ellipsoidal inclusions is [1, 28],

$$\varepsilon_{eff} = \varepsilon_b + \frac{\frac{1}{3}\sum_{i=1}^{n} f_i\left(\varepsilon_i - \varepsilon_b\right)\sum_{k=1}^{3}\frac{\varepsilon_b}{\varepsilon_b + N_{ik}(\varepsilon_i - \varepsilon_b)}}{1 - \frac{1}{3}\sum_{i=1}^{n} f_i\left(\varepsilon_i - \varepsilon_b\right)\sum_{k=1}^{3}\frac{N_{ik}}{\varepsilon_b + N_{ik}(\varepsilon_i - \varepsilon_b)}} \tag{C1}$$

where $\varepsilon_{b,i} = \varepsilon_{i,b\infty} + \chi_{i,b}(\omega)$ are the relative permittivities of the base material and of the i-th type of inclusions, respectively. In the general case, they are complex and depend on frequency. In (C1), f_i is the volume fraction occupied by the inclusions of the i-th type; N_{ik} are the depolarization factors [25, 29] of the i-th type of inclusions, where indices $k = 1, 2, 3$ corresponds to x, y, and z coordinates. If the inclusions are thin cylinders, their two depolarization factors are close to 1/2, and the third can be calculated as in [30], $N \approx (a)^{-2}\ln(a)$, where $a = l/d$ is a cylinder's aspect ratio (length/diameter). The sum of all three depolarization factors is always unity. Since the MG formula is linear, the resultant effective permittivity of the mixture can be also represented through effective high-frequency permittivity and susceptibility function [29],

$$\varepsilon_{eff} = \varepsilon_{eff\,\infty} + \chi_{eff}(\omega). \tag{C2}$$

If inclusions are conducting (metallic), their frequency-dependent relative permittivity is

$$\varepsilon_i(j\omega) = \varepsilon' - j\varepsilon'' = \varepsilon' - i\sigma/\omega\varepsilon_0. \tag{C3}$$

The MG mixing rule is applicable when the concentration of the conducting particles in the mixture is below the percolation threshold. The percolation concentration can be evaluated as $p_C = C/a$, where a is an aspect ratio for the inclusions, and C is the experimental coefficient depending on the technology of the composite manufacturing (typically, $1 \le C \le 10$) [31].

When concentration of inclusions is higher than the percolation threshold, the different approximations from the general effective medium theories should be used, for example, McLachlan [32] or Ghosh-Fuchs approximations [33]. The McLachlan's equation is used to describe effective parameters of the mixture close to or above the percolation threshold is [32, 34].

$$\frac{(1-f_i)\left(\varepsilon_b^{1/s} - \varepsilon_{eff}^{1/s}\right)}{\varepsilon_b^{1/s} + \left(\frac{1-p_c}{p_c}\right)\varepsilon_i^{1/s}} + \frac{f_i\left(\varepsilon_i^{1/t} - \varepsilon_{eff}^{1/t}\right)}{\varepsilon_i^{1/t} + \left(\frac{1-p_c}{p_c}\right)\varepsilon_{eff}^{1/t}} = 0. \tag{C4}$$

In (C4), the values s and t are the process exponents [34]. Their ratio s/t determines the symmetry of the real and imaginary part of the permittivity around the percolation threshold.

REFERENCES

1. Huang, J. Y., P. C. Ravva, M. Y. Koledintseva, R. E. DuBroff, J. L. Drewniak, B. Archambeault, and K. N. Rozanov, "Design of a metafilm-composite dielectric shielding structure using a genetic algorithm," *Proc. Progress In Electromagnetic Research Symposium (PIERS 2006 Cambridge)*, 297–301, Cambridge, MA, USA, March 26–29, 2006.
2. Koledintseva, M. Y., P. C. Ravva, R. E. DuBroff, J. L. Drewniak, K. N. Rozanov, and B. Archambeault, "Engineering of composite media for shields at microwave frequencies," *Proc. IEEE Symp. Electromag. Compat.*, Vol. 1, 169–174, Chicago, IL, August 2005.
3. Paris, D. T., "Computer aided radome analysis," *IEEE Trans. Ant. Propag.*, Vol. 18, 7–15, 1970.
4. Felsen, L. B. and N. Marcuvitz, *Radiation and Scattering of Waves*, Vol. 2, Prentice-Hall, Englewood Cliffs, N.J., 1973.
5. Chew, W. C., *Waves and Fields in Inhomogeneous Media*, Van Nostrand Reinhold, New York, N.Y., 1990.
6. King, R. W. P., "The electromagnetic field of a horizontal electric dipole in the presence of a three-layered region," *J. Appl. Phys.*, Vol. 69, No. 12, 7987–7995, June 1991.
7. King, R. W. P., "The electromagnetic field of a horizontal electric dipole in the presence of a three-layered region: Supplement," *J. Appl. Phys.*, Vol. 74, No. 8, 4845–4848, October 1993.
8. King, R. W. P., M. Owens, and T. T. Wu, *Lateral Electromagnetic Waves: Theory and Applications to Communications, Geophysical Exploration, and Remote Sensing*, Springer-Verlag, April 1992.
9. Zhang, H.-Q., W.-Y. Pan, K. Li, and K.-X. Shen, "Electromagnetic field for a horizontal electric dipole buried inside a dielectric layer coated high lossy half space," *Progress In Electromagnetics Research*, PIER 50, 163–186, 2005.
10. Li, K. and Y.-L. Lu, "Electromagnetic field from a horizontal electric dipole in the spherical electrically earth coated with N-layered dielectrics," *Progress In Electromagnetics Research*, PIER 54, 221–244, 2005.
11. Bodrov, V. V. and I. V. Sourkova, "The effect of multilayered dielectric radomes with different shapes on the amplitude

and phase characteristics of antennas with planar aperture," *Proc. URSI Int. Symp. Electromagnetics Theory*, 391–393, St. Petersburg, May 1995.

12. Bodrov, V. V. and I. V. Sourkova, "Effect of a multilayered cylindrical dome on the pattern of an antenna array arranged arbitrarily with respect to the dome," *J. Communications Technology and Electronics*, Vol. 40, No. 7, 91–97, 1995.
13. Bodrov, V. V., I. V. Sourkova, and V. I. Sourkov, "Effect of a multilayered spherical dome on the amplitude and phase characteristics of the system of radiators arranged arbitrarily with respect to the dome," *J. Communications Technology and Electronics*, Vol. 42, No. 2, 1997.
14. Sabirov, M., I. Sourkova, V. Sourkov, V. Bodrov, and M. Koledintseva, "Power characteristics of radiators in multilayered dielectric structures," *Progress In Electromagnetics Research Symposium, PIERS-04*, 409–412, Pisa, Italy, March 28–31, 2004.
15. Stratton, J. A., *Electromagnetic Theory*, McGraw-Hill, New York, London, 1941.
16. Pozar, D. M., *Microwave Engineering*, John Wiley, New York, NY, 1998.
17. Derat, B. and J.-C. Bolomey, "Analytical lower and upper bounds of power absorption in near-field regions deduced from a modal-based equivalent junction model," *Progress In Electromagnetics Research*, PIER 58, 21–49, 2006.
18. Paul, C. R., *Introduction to Electromagnetic Compatibility*, John Wiley, New York, NY, 1992.
19. Neelakanta, P. S., *Handbook of Electromagnetic Materials*, CRC Press, Boca Raton, FL, 1995.
20. Kuester, E. F. and C. L. Holloway, "Comparison of approximations for effective parameters of artificial dielectrics," *IEEE Trans. Microw. Theory Techn.*, Vol. 3, 1752–1755, 1990.
21. Sheng, P., "Theory of dielectric function of granular composite media," *Phys. Rev. Letters*, Vol. 45, No. 1, 60–63, 1980.
22. Doyle, W. T. and I. S. Jacobs, "The influence of particle shape on dielectric enhancement in metal-insulator composites," *J. Appl. Phys.*, Vol. 71, No. 8, 3926–3936, 1992.
23. Diaz, R. E., W. M. Merrill, and N. G. Alexopoulos, "Analytical framework for the modeling of effective media," *J. Appl. Phys.*, Vol. 84, No. 12, 8615–6826, 1998.
24. Garnett, J. C. M., "Colors in metal glasses and metal films," *Philos. Trans. R. Soc.*, Sect. A, Vol. 3, 385–420, London, 1904.

25. Sihvola, A., "Effective permittivity of dielectric mixtures," *IEEE Trans. Geosc. Remote Sens.*, Vol. 26, No. 4, 420–429, 1988.
26. Sihvola, A., *Electromagnetic Mixing Formulas and Applications*, The IEE, London, UK, 1999.
27. Sihvola, A., "Metamaterials and depolarization factors," *Progress In Electromagnetics Research*, PIER 51, 65–82, 2005.
28. Koledintseva, M. Y., R. E. DuBroff, and R. W. Schwartz, "A Maxwell Garnett model for dielectric mixtures containing conducting particles at optical frequencies," *Progress In Electromagnetics Research*, PIER 63, 223–242, 2006.
29. Koledintseva, M. Y., J. Wu, J. Zhang, J. L. Drewniak, and K. N. Rozanov, "Representation of permittivity for multi-phase dielectric mixtures in FDTD modeling," *Proc. IEEE Symp. Electromag. Compat.*, Vol. 1, 309–314, Santa Clara, CA, Aug. 9–13, 2004.
30. Matitsine, S. M., K. M. Hock, L. Liu, et al., "Shift of resonance frequency of long conducting fibers embedded in a composite," *J. Appl. Phys.*, Vol. 94, No. 2, 1146–1154, 2003.
31. Lagarkov, A. N. and A. K. Sarychev, "Electromagnetic properties of composites containing elongated conducting inclusions," *Physical Review B*, Vol. 53, No. 10, 6318–6336, March 1996.
32. McLachlan, D. S., A. Priou, I. Chernie, E. Isaac, and E. Henry, "Modeling the permittivity of composite materials with general effective medium equation," *J. Electromagn. Waves and Applications*, Vol. 6, No. 6, 1099–1131, 1992.
33. Ghosh, K. and R. Fuchs, "Spectral theory for two-component porous media," *Phys. Review B*, Vol. 38, 5222–5236, 1988.
34. Youngs, I. J., "Exploring the universal nature of electrical percolation exponents by genetic algorithm fitting with general effective medium theory," *J. Phys, D: Appl. Phys.*, Vol. 35, 3127–3137, 2002.